Cell-targeted dendrimer-norketamine nanomedicine for neuroprotection in experimental *status epilepticus*

Preeti Vyas[1#], Wathsala Liyanage[2#], Javier Allende Labastida[1], James L. Sowers[1], Milan Paul[2], Bruno Henrique Dallo Gallo[3], Susanna Scafidi[1], Kavichandhirakanth Murugesan[2], Kathleen Lac[1], Lirong Shao[3], Narendra Kale[2], Maria Paula Avalos[1], Carl E. Stafstrom[3], Kunal S. Parikh[2], Rangaramanujam M. Kannan[2*], Sujatha Kannan[1*]

[1] Department of Anesthesiology and Critical Care Medicine, JHU SOM, Baltimore, MD

[2] Center for Nanomedicine, Department of Ophthalmology, Wilmer Eye Institute, JHU SOM, Baltimore, MD

[3] Department of Neurology, JHU SOM, Baltimore, MD

#equal contribution

***Corresponding authors**

Sujatha Kannan, MD, Professor, Anesthesiology and Critical Care Medicine, Johns Hopkins University School of Medicine, Baltimore, MD 21231, USA

Tel: +1 410-955-6412; email: skannan3@jhmi.edu

ORCID ID: 0000-0002-9497-5786

Rangaramanujam M. Kannan, Ph.D., Arnall Patz Distinguished Professor of Ophthalmology, Center for Nanomedicine, Wilmer Eye Institute, Johns Hopkins University School of Medicine, 400 N. Broadway, Baltimore, MD 21231, USA.

Tel.: +1 443-287-8634; Fax: +1 443-287-8635; e-mail: krangar1@jhmi.edu

ORCID ID: 0000-0002-3712-7836

Abstract

Rationale: *Status epilepticus* (SE) is a neurological emergency with limited therapeutic options, often resulting in death or severe neurodegeneration in survivors. Although ketamine is increasingly used for refractory SE, its clinical utility is restricted by sedation, respiratory depression, rapid hepatic metabolism, and off-target central nervous system effects. We developed a glucose dendrimer–norketamine conjugate (GD-Ket) to selectively target hyperactive neurons while improving efficacy and safety.

Methods: GD-Ket was synthesized by conjugating approximately seven molecules of norketamine to a glucose dendrimer through stable amide linkages. The conjugate was characterized using NMR, HPLC, dynamic light scattering, and zeta potential analysis. GD-Ket labeled with Cy5 was used to assess cellular localization *in vitro* and *in vivo*. Pharmacological activity, biodistribution, metabolic stability, and safety were assessed *in vitro* and *in vivo*, as well as short- and long-term efficacy, in a pilocarpine-induced mouse model of SE.

Results: GD-Ket significantly improved survival and protected against SE in male and female mice at a fraction of the ketamine dose typically used in the pilocarpine-induced SE model. Approximately 73% of mice treated with GD-Ket recovered from SE within the first hour, whereas none recovered with ketamine or saline. A single dose of GD-Ket decreased neuronal injury and inflammation at 48 h and improved long-term neurobehavioral deficits at 4 months post-SE. GD-Ket localized intracellularly in neurons *in vitro* and *in vivo* and exerted its intracellular neuroprotective effect *via* modulation of sigma chaperones. Importantly, unlike ketamine, GD-Ket was not metabolized by liver enzymes and showed no *in vitro* toxicity or adverse effects, such as sedation or fatal respiratory depression *in vivo*, even at 1,000x the therapeutic dose.

Conclusion: GD-Ket substantially expands the therapeutic index of ketamine by combining pathology-specific delivery with dual intracellular and receptor-mediated mechanisms. This first-

in-class dendrimer nanotherapy safely arrests established SE while providing durable neuroprotection, supporting its clinical translation for *SE* and other neurological disorders.

Keywords: Ketamine, Glucose dendrimers, Nanomedicine, *Status epilepticus*, Precision therapeutics

Introduction

Ketamine is primarily recognized for its role as a dissociative anesthetic, acting as a non-competitive antagonist at open-channel *N*-methyl-D-aspartate (NMDA) receptors. However, it also serves as an allosteric modulator of the NMDAR when the channel is closed [1]. Ketamine's neuroprotective effects have been attributed to its antagonism of synaptic and extrasynaptic NMDARs [2–4]. Unlike other more potent NMDAR antagonists, ketamine's affinity for NMDAR is in the μM range; therefore, ketamine's broad efficacies may be exerted through multiple mechanisms including its action on opiate [5] and sigma (σ) receptors [6]. Owing to its wide-ranging neuroprotective actions, ketamine is currently being evaluated in several CNS disorders including refractory epilepsy [7], chronic pain [8], refractory depression [9] and Rett syndrome [10]. However, its use is limited to highly controlled settings due to debilitating side effects including hallucinogenic and psychomimetic effects, high risk for drug abuse in the short term, cognitive impairment, and decline in executive functioning with chronic exposure. Additionally, the possibility of fatal respiratory depression at higher doses restricts its applications despite ketamine's promising therapeutic potential in various disorders [11–13].

Recently, ketamine has been used as a continuous infusion for treatment of *status epilepticus* (SE) and refractory *status epilepticus* (RSE) in critical care settings [7]. SE is a medical and neurological emergency characterized by self-sustaining, continuous, or recurring seizures, leading to neuroinflammation, neurodegeneration, and abnormal neurogenesis [14]. Approximately 43% of patients with SE admitted to the hospital develop RSE [15], with in-hospital mortality rates as high as 40-54%. Little progress has been made in developing therapies for the acute management of SE and RSE [15]. NMDARs are critical in initiating and maintaining SE, signifying the therapeutic potential of ketamine as an anti-seizure medication (ASM) [16]. Preclinical studies have shown that ketamine is effective in pilocarpine-induced animal models of SE at doses ranging from 10-25 mg/kg [17]; however, these doses have been associated with

respiratory depression, dose-dependent neuronal injury, and apoptosis [11]. These side effects are commonly seen with NMDAR antagonists and are rate-limiting factors in the clinical development of NMDAR-targeted ASMs.

Building on our previous research on microglia-targeted hydroxyl polyamidoamine (PAMAM) dendrimers that attenuated neuroinflammation in multiple models of brain injury and are currently advancing through Phase 2 clinical trials [18,19]; and aligned with previous studies by us [20] and others [21,22], we leveraged glucose conjugation for improved brain penetration and developed non-degradable dendrimers constructed mainly from glucose building blocks (GD). Upon systemic administration, GDs specifically target metabolically stressed neurons and glia. We have previously shown that our glucose dendrimers promote cellular uptake *via* multivalent surface interactions with glucose transporters without providing metabolizable glucose to cells [20]. In this study, we demonstrate that glucose dendrimers, when conjugated to racemic norketamine – the major active metabolite of ketamine, preserve the binding affinity to NMDAR while also acting on intracellular σ receptors. Our results demonstrate that systemic administration of dendrimer-norketamine (GD-Ket) *via* the intraperitoneal (IP) route crosses the blood-brain barrier, accumulates in hippocampal neurons, reduces inflammation and cell death, and significantly increases survival, with sustained efficacy in controlling generalized seizures and arresting SE in this model. A single dose of GD-Ket also preserved long-term behavior; it reduced hyperactivity and preserved motor coordination 4 months post-SE in treated animals. Notably, GD-Ket demonstrated an exceptional safety profile even at 1,000x the therapeutic dose, while free ketamine was lethal at these doses. These results significantly broaden the therapeutic index of ketamine for clinical translation and build on the promise of dendrimers for clinical use.

Results

Synthesis, characterization and NMDAR binding affinity of GD-Ket conjugates

GD-Ket was synthesized using second-generation glucose dendrimers (GD2) [20,23] and (R, S)-Norketamine – the major active metabolite of ketamine. The norketamine used for conjugation is a racemic mixture containing equal parts of (R)- and (S)-norketamine. The amine group of (R, S)-Norketamine **(1)** was reacted with azido-PEG_4-NHS in DCM at room temperature for 12 h to yield (*R, S*)-Norketamine-PEG_4-azide **(2) (Figure 1A)**. The ^{1}H NMR spectrum of compound **2** showed PEG protons at δ 4.2 ppm and aromatic protons at δ 7.5-8 ppm. GD2 was partially functionalized with approximately 7 acetylene groups using NaH and propargyl bromide under these conditions for subsequent click reactions. (R, S)-Norketamine-PEG4-azide was then conjugated to GD2 *via* a Cu(I)-catalyzed click (CuAAC) reaction that occurs with a catalytic amount of $CuSO_4$•$5H_2O$ and sodium ascorbate to form the GD-Ket drug conjugate (GD-Ket). The crude product was dialyzed using a 1 KDa membrane against *N,N*-dimethylformamide (DMF) for 12 h to remove low-molecular-weight impurities. Copper traces were removed by dialysis with EDTA, followed by dialysis in ultrapure water for 24 h (Figure 1B)**.** The final product, GD-Ket, was characterized using ^{1}H NMR (DMSO-*d6*). The 1H NMR spectrum of GD-Ket showed a signal indicative of triazole protons from the glucose dendrimer at δ 7.8-8.2 ppm (as a multiplet) and the triazole peak for (*R,S*)-Norketamine-PEG_4-azide at δ 7.49 ppm (as a singlet), along with norketamine aromatic protons at δ 7.38-7.19 ppm and norketamine cyclohexanone peaks at δ 2.21-1.06 ppm **(Figure 1C)**.

Analytical reversed-phase High-Performance Liquid Chromatography (HPLC) was used to assess product purity. The comparative HPLC chromatograms of the GD2 dendrimer, norketamine, and GD-Ket showed evident shifts in retention times at 210 nm **(Figure 1D)**. The drug loading on GD-Ket was calculated to be 10% by weight, as determined by ^{1}H NMR. The drug loading on GD-Ket was calculated to be 10% by weight, as determined by ^{1}H NMR. The mean hydrodynamic diameter and zeta potential of GD-Ket were 4.2 ± 2 nm (**Figure 1E**) and -0.41 ± 0.17 mV (**Figure S1)**, respectively.

The NMDAR1A/2B antagonist activity of GD-Ket was evaluated by Eurofins DiscoverX using the SAFETYscan E/IC50 ELECT ion channel assay using cells expressing the human NMDAR1A/2B ion channel. Changes in ion channel activity were measured using a FLIPR Tetra® fluorescence plate reader, and concentration-response curves were generated to determine IC_{50} values by nonlinear regression. The IC_{50} of GD-Ket (on a conjugate basis) was >10 times lower than that of norketamine, indicating that the GD-Ket conjugate is functionally much more potent than the norketamine that was conjugated to the dendrimer **(Figure 1F)**. This is likely due to the higher affinity of the conjugate with 7 molecules of norketamine conjugated to each GD2 molecule.

The drug is attached to the dendrimer using a stable amide bond. The stability of this conjugation was assessed using *in vitro* drug release studies of GD-Ket under both intracellular and extracellular conditions. GD-Ket was incubated at a physiological temperature of 37 °C in two distinct buffer systems: a sodium citrate buffer at pH 5.5, containing esterase to simulate the acidic environment of lysosomes, and phosphate-buffered saline (PBS) at pH 7.4 to represent plasma conditions. The release of ketamine was minimal in both conditions, with less than 5% released over 4 days (100 h) **(Figure 1G)**. This demonstrates that the conjugate is stable under both intracellular and plasma-like conditions, thereby minimizing drug release and remaining active without releasing the conjugate. The minimal release of ketamine (<5% over 4 days) demonstrates that the dendrimer–ketamine conjugate is highly stable under physiological conditions, indicating that the observed therapeutic effects are primarily mediated by the intact conjugate rather than by released free ketamine. This interpretation is supported by our previous dendrimer–MK-801 study, which demonstrated therapeutic efficacy despite negligible drug release, suggesting that the intact dendrimer–drug conjugate is the pharmacologically active species [24,25].

Biodistribution and metabolic stability of GD-Ket show rapid elimination from circulation and no metabolism in the liver

In vivo imaging was performed using IVIS following systemic administration of Cy5-labeled GD-Ket (Cy5-GD-Ket), and biodistribution was compared between control and pilocarpine-induced SE mice **(Figure 2A-C)**. Most of the Cy5-GD-Ket was eliminated from the WT mice within the first 12 h, while a sustained signal was noted even at 72 h in the whole body ($p<0.0001$) **(Figure 2B)** as well as in the micro-dissected SE brains **(Figure 2C)**. There was no measurable signal noted in the different regions of the micro-dissected WT brain; however, we observed region-specific accumulation of Cy5-GD-Ket 72 h post-injection in SE mice, suggesting greater uptake of GD-Ket in brain areas most involved in seizure activity and inflammation. We observed a significant accumulation of GD-Ket in the hippocampus, cortex, thalamus, and striatum, which are critical sites of seizure generation, propagation, and modulation in this model. **(Figure 2C, S2)**. We also detected a high signal in the cerebellum, which has a high density of granule cells; however, the intracellular uptake of GD-Ket was confirmed in the hippocampal-cortical-thalamic axis of seizing mice using confocal microscopy. This shows that the distribution of Cy5-GD-Ket is pathology-mediated, both *in vitro* and *in vivo*. GD-Ket targets the brain regions associated with seizures in SE but not healthy mice for 72 h post-injury **(Figure S2)**. A higher whole-body signal on IVIS and increased accumulation in the liver are observed in SE mice compared with WT healthy mice, which may be due to a higher metabolic rate driven by active seizures.

We assessed the metabolic stability of GD-Ket conjugate versus free ketamine and free norketamine *in vitro* using human liver microsomes. HPLC analysis confirmed that free ketamine and norketamine are rapidly metabolized within 4 h. In contrast, GD-Ket was not metabolized by human liver microsomes, demonstrating enhanced stability **(Figure 2D-E)**. This demonstrates that dendrimer conjugation prevents hepatic enzymatic degradation and subsequent toxic effects of the metabolites. **(Figure 2D-E, Figure S3)**. GD conjugation reduces ketamine metabolism and protects it from Phase I enzymatic degradation, thereby improving stability without the formation

or accumulation of active metabolites. These data are also consistent with the stability data indicating that GD-Ket is not metabolized and that ketamine is not released to a substantial extent from the conjugate, as seen in the release studies in **Figure 1H**. A calibration curve was established to enable quantitative conversion of fluorescence intensity into drug concentration, ensuring accurate analysis of tissue biodistribution. This approach provides a standardized method for quantifying GD-ketamine from fluorescence measurements and strengthens the interpretation of biodistribution data. The calibration curve also supports a correlation between fluorescence-based imaging and quantitative drug levels, thereby improving the reliability and reproducibility of pharmacokinetic and tissue distribution analyses **(Figure S4).**

GD-Ket localizes in neurons and microglia upon systemic delivery in a mouse model of pilocarpine-induced SE

Pilocarpine-induced seizures severely affect the hippocampus, where muscarinic receptors are abundant, followed by the cortex and thalamus [26]. The red nucleus area is critical in seizure propagation and increases the risk of recurrent SE, making it an important region in the long-term propagation and maintenance of seizures [27]. Regional and cellular localization of Cy5-GD-Ket in SE was determined by confocal imaging that showed the presence of Cy5-GD-Ket in the pyramidal cell layer of the CA3 and DG regions of the hippocampus, along with the thalamus, cortex, and red nucleus in the midbrain **(Figure 3A-B, S5)**. This demonstrates that the neuronal localization of Cy5-GD-Ket follows seizure propagation. We also observed localization of Cy5-GD-Ket in microglia in the hippocampus **(Figure 3C)**, an area involved in neuroinflammation post-SE.

Acute GD-Ket treatment attenuates seizure severity, improves survival, and preserves long-term behavior in pilocarpine-induced SE

Acute seizures: We evaluated the efficacy of GD-Ket using a well-established *in vivo* model of pilocarpine-induced SE [28]. All efficacy comparisons were made with ketamine, which is used clinically for treatment of SE in critical care settings. To mimic clinical scenarios, treatment was initiated 15 mins after SE induction with pilocarpine. Mice were treated with either saline, ketamine IP (0.3 mg/kg), or GD-Ket IP (0.3 mg/kg based on norketamine) **(Figure 4A-B)**. The dose was based on our pilot data, in which 0.3, 3, and 30 mg/kg IP of GD-Ket showed similar anti-seizure responses **(Figure S6A-E)** in the first 120 min against pilocarpine-induced behavioral SE ($p = 0.0074$, $F(3,7) = 12.26$). We selected the lowest efficacious dose of GD-Ket (0.3 mg/kg IP) for *in vivo* efficacy studies. In this mouse model, GD-Ket administered at a low dose resulted in a substantial decrease in mortality within the initial 48 h following the SE **(Figure 4C)**, which corresponds to the peak phase of acute excitotoxicity and systemic physiological stress in this model [29–32]. We observed survival rates of 44.4% with saline, 46.0% with ketamine 0.3 mg/kg IP, and 77.3% with GD-Ket 0.3 mg/kg IP **(Figure 4D)**. All animals were included in the survival studies. Previous studies have demonstrated that SE-induced mortality typically plateaus within 48 h; therefore, survival at this time point is a reliable indicator of the immediate neuroprotective and life-saving potential of GD-Ket [29]. Only the mice that survived the entire 120-min observation period were included in the behavioral seizure scoring analysis.

With GD-Ket therapy, we observed a significant decrease in the duration of higher stages on the modified Racine scale [28,33], particularly stages 4-6 **(Figure 4E, Figure 65H-J).** The saline-treated mice quickly progressed from 4 to 6, and this group demonstrated higher mortality. With GD-Ket treatment, less than 20% of the total seizure duration was medium (stage 3-4) or high-grade (stage 5-6), and less than 5% of total time was spent in high-grade seizures, unlike saline-treated and free-ketamine-treated animals **(Figure 4E-F).** The effect of GD-Ket IP is sustained over time (**Figure 4G).** The overall high-grade seizure burden (stage 3-6) was significantly lower upon treatment with GD-Ket ($p < 0.01$, $F(3.897, 163.7) = 5.046$) when compared to saline- or free

ketamine treated animals (**Figure 4G, Figure S6).** This indicates that SE was rapidly controlled with GD-Ket treatment, with either cessation of clinical seizures or a decrease to unsustained low-grade seizures that are usually not associated with ongoing pathology and high morbidity or mortality. Approximately 73% of GD-Ket IP-treated animals recovered from SE within the first hour of treatment, while none of the free ketamine or saline-treated animals recovered in this time **(Figure 4H).** Free ketamine IP at a dose of 0.3mg/kg was ineffective and did not significantly reduce mortality compared with saline. This is consistent with previous literature where the effective dose of ketamine in a mouse model of pilocarpine-induced SE was 10-25 mg/kg IP [17]. GD alone had no anti-seizure effect **(Figure S6K)** p=0.7615, F (DFn, Dfd) = 2.615(3,8)), indicating that the therapeutic efficacy is due to the conjugated drug rather than the dendrimer itself. We also assessed potential sex-dependent differences. Female mice demonstrated comparable therapeutic efficacy following pilocarpine challenge, consistent with observations in the male cohorts **(Figure S7).**

Continuous EEG monitoring with power spectral analysis was also performed in representative male mice to correlate clinical behavioral findings with the EEG ($n = 3$ n per group, **Figure S8**). Baseline recordings following pilocarpine administration confirmed sustained electrographic SE, characterized by persistent high-frequency, high-amplitude ictal spike discharges and a pronounced surge in total EEG signal power. GD-Ket treatment reduced total power across major frequency bands, returning toward baseline levels (**Figure S8),** confirming that electrographic SE was terminated in the pilocarpine model and that this correlated with clinical seizures**.** This shows that selective delivery of ketamine by GD at the site of injury enables sustained efficacy at a much lower dose than typically used.

***Long-term behavior*:** We evaluated the long-term neuroprotective efficacy of acute GD-Ket therapy against pilocarpine-induced chronic neurobehavioral deficits 4 months post-SE. Untreated controls exhibited a hyperactive phenotype in the open field test, with significantly

elevated mean and maximum velocities and total distance traveled **(Figure 4I-K),** as further confirmed by an increased number of line crossings during the 10-minute test period **(Figure S9A).** Conversely, acute administration of GD-Ket significantly attenuated this hyperactivity, normalizing both mean and maximum velocities and line-crossing frequency**,** unlike the saline- and ketamine-treated groups **(Figure 4I-J)**. A single dose of GD-Ket also decreased the total distance traveled in the open field, indicating normalization of hyperactive behavior 4 months post-SE. Animals treated with saline or ketamine also showed a clear behavioral difference in anxiety-like traits, spending less time in the center than at the periphery, consistent with a typical anxiety pattern previously reported **(Figure 4K-L, Figure S9B-E)** [34]**.** GD-Ket treatment markedly increased the center-to-periphery ratio **(Figure 4K),** indicating a dramatic reduction in anxiety-like behavior that was not achieved by standalone ketamine or saline controls. Our data suggest that a single dose of GD-Ket treatment during SE can effectively reverse chronic hyperactivity and anxiety-like behavior 4 months post-SE **(Figure S8C-G).**

Both the Pilo/Sal and Pilo/Ket cohorts demonstrated severe impairment in motor coordination, marked by a progressive failure to balance on the rotarod for three trials. While several prior studies with early chronic timelines (1–2 months post-SE) report spared rotarod performance [34], our evaluation at 4 months post-SE revealed a pronounced motor coordination deficit, indicating a loss of baseline motor function. In addition to the neurobehavioral deficit, our long-term data show progressive injury in the pilocarpine model, in which widespread extra-limbic neurodegeneration extends well beyond classical temporal structures. Additionally, the potential contribution of systemic chronic frailty, muscle weakness, or post-ictal exhaustion from recent unobserved seizures must be considered as compounding factors in our long-term chronic cohorts. Interestingly, mice treated with GD-Ket exhibited preserved motor coordination, with significantly higher fall latency compared to both saline ($p < 0.05$) and free ketamine ($p < 0.0001$)

mice (**Figure 4M).** These data demonstrate that GD-Ket provides superior long-term protection against chronic locomotor and motor deficits over free ketamine.

GD-Ket protects against neuronal cell death and hippocampal inflammation associated with pilocarpine-induced SE

Permanent neurological damage and neuronal death can occur within 30 min of convulsive SE. Published data indicate the presence of FluoroJade C (FJC)-positive degenerating neurons starting at 4 h, peaking at 12-72 h, and gradually decreasing at 1-2 weeks after pilocarpine-induced SE [35]. In chemoconvulsant-induced SE models (pilocarpine and kainate), microglia are activated within the first few h of SE and contribute to pathogenesis by releasing pro-inflammatory cytokines that lower the threshold for subsequent seizures [36]. Degenerating neurons and activated glia, particularly in the hippocampus, trigger inflammatory mechanisms and play a crucial role in the neuropathology and pathophysiology that promote epileptogenesis, as seen in patients [35,37]. We evaluated the efficacy of GD-Ket versus saline-treated brain tissue after 48 h. Because the equivalent dose of free ketamine has historically not shown efficacy against resistant seizures [17], we did not include 0.3 mg/kg IP ketamine therapy in the histological assessments for comparison with GD-Ket therapy.

Immunohistochemistry of the brain sections demonstrates that pilocarpine-induced SE resulted in degenerative death of neuronal cells, primarily in CA1 and DG regions of the hippocampus, 48 h post-SE, as shown by increased FJC-stained neurons **(Figure 5A-B)**. Quantitative analysis indicated a significant decrease in FJC-positive neurons with ketamine and GD-Ket, with a greater decrease in degenerating neurons in the GD-Ket groups **(Figure 5C)**. Increased neuronal death was observed in the CA1, CA3, and DG regions of the hippocampus, which was reduced by IP administration of GD-Ket. This neuronal cell death, coupled with hyperactivity, frequently results in elevated levels of brain-derived neurotrophic factor (BDNF) mRNA and protein in the hippocampus and cortical regions. It contributes to abnormal circuit formation in the brain,

including mossy fiber sprouting, which is implicated in epileptogenesis. We observed an increase in BDNF levels in the hippocampus ($p<0.0001$, $F(3, 18) = 18.92$) and cortex 48 h after pilocarpine-induced SE ($p<0.0001$, $F(3, 18) = 29.70$), which was reduced by GD-Ket treatment. GD-Ket demonstrated superior efficacy compared to ketamine ($p < 0.001$). We observed microglial activation **(Figure 5D)** and a change in microglial morphology to a rod-shaped, bushy, and hypertrophic phenotype. We also observed increased microglial density in saline and free ketamine mice with pilocarpine-induced SE, and decreased microglial density and microglial morphology, with predominantly ramified microglia, in the GD-Ket groups at 48 h post-SE **(Figure 5E)**. This was accompanied by a decrease in TNF-α ($p = 0,03$, $F(3, 19) = 8.639$), IL-1β ($p = 0.032$, $F(3, 19) = 6.112$) and IL-6 ($p = 0.002$, $F(3, 20) = 11.93$) levels with 0.3 mg/kg of GD-Ket, while free ket at this dose was ineffective in decreasing inflammation **(Figure 5F-H)**.

GD-Ket localizes intracellularly and demonstrates non-NMDAR effects through modulation of receptor σ chaperone protein

The primary effects of ketamine *via* blockade of the NMDA receptor have been extensively studied. Accumulating evidence shows that ketamine can also exert effects *via* non-NMDAR mechanisms, including intracellular interactions with both σ receptor chaperone proteins, regulating calcium signaling, ion channels, and inflammation, and triggering alterations in BDNF levels [16] [38]. We evaluated the intracellular localization of GD-Ket and its effect on σ receptor modulation *in* differentiated HT-22 cells *in vitro*.

In line with our *in vivo* data, we show that GD-Ket localizes intracellularly in differentiated HT-22 neurons exposed to glutamate excitotoxicity **(Figure 6A).** Fluorescent signals were predominantly observed in the perinuclear region and along neurites, suggesting targeted uptake by metabolically active and hyperexcitable neurons. Quantitative analysis also confirmed a significant increase in Cy5-GD-Ket uptake intracellularly in glutamate-exposed cells when

compared to healthy neurons, confirming that glutamate exposure leads to increased intracellular uptake of the GD (***p < 0.001, F (DFn, Dfd) = 3.465 (10, 10)).

Given robust intracellular localization of GD-Ket in both *in vivo* and *in vitro settings*, we tested whether GD-Ket exerts non-NMDAR effects by modulating σ1 receptors. Here, we show that glutamate exposure significantly increases inflammatory protein levels, and that administration of GD-Ket reduces these levels **(Figure 6B, C1-3)**. Unlike ketamine, pretreatment with the σ antagonist BD-1047 (3nM, which primarily inhibits σ1 at this dose) before GD-Ket reversed the neuroprotective and anti-inflammatory effects of GD-Ket. In the presence of BD-1047, σ1 receptors were already blocked when differentiated hippocampal neurons were exposed to GD-Ket; therefore, it could not reduce the levels of cytokines, BDNF, or Nerve growth factor (NGF) **(Figure 6).** Inhibition of σ1 with BD-1047 had no effect on free ketamine action, indicating that intracellular σ1R (non-NMDAR) does not play a significant role in the mechanism of action of free ketamine, unlike GD-Ket. These data indicate that GD-Ket accumulates intracellularly, exerting part of its neuroprotective and anti-inflammatory effects *via* non-NMDAR mechanisms, such as modulation of intracellular σ chaperone proteins.

GD-Ket shows no *in vitro* or *in vivo* toxicity, unlike free ketamine at equivalent doses

Ketamine has previously been shown to induce mitochondrial stress and reduce ATP production, even at a lower dose of 100 μM, without associated cell death or caspase activation [39]. We evaluated mitochondrial respiration in HT-22 cells after exposure to ketamine or GD-Ket. We show that 100 μM ketamine (~23 μg/mL) decreased the oxygen consumption rate, with significant reductions in basal respiration (p=0.0033), maximal respiration (p=0.0034), and spare respiratory capacity ratio (p=0.0301) compared with saline control. In contrast, basal respiration, maximal respiration, and spare respiratory capacity following treatment with GD alone or GD-Ket at equivalent ketamine doses were similar to saline-treated controls and significantly better than with ketamine treatment **(Figure 7A1-A4)**. These results show that both GD alone and GD-Ket did not

affect mitochondrial function or health, indicating they are not cytotoxic, unlike free ketamine treatment, which impairs mitochondrial function.

We further explored the safety of GD and GD-Ket in the *in vivo* experiments. In line with previous studies [40], our *in vivo* safety studies in healthy C57Bl/6 mice with systemic free ketamine administration showed a dose-dependent sedative effect. Intraperitoneal (IP) administration of 75 mg/kg of ketamine led to decreased mobility, irregular breathing, and respiratory distress. At 100 and 300 mg/kg doses, systemic ketamine caused deep sedation with severe respiratory depression, leading to death within 7 min at 300 mg/kg. However, GD-Ket demonstrated no sedative effects even at 300 mg/kg IP. Unlike free ketamine, GD-Ket administration did not lead to lack of coordination, immobility, sedation, or respiratory depression, even at 300 mg/kg IP **(Video S1),** either acutely or in a delayed manner, demonstrating the safety of GD-Ket across a wide range of doses **(Figure 7B1- B3)**. This is seen despite the lower IC_{50} of GD-Ket, indicating that selective targeting of this dendrimer platform has the potential to deliver ketamine specifically to the site of pathology (i.e., injured neurons), avoiding the non-specific CNS side effects of ketamine and increasing the safety margin.

Materials and Methods

Synthesis

The synthesis of compound 3, the GD2 dendrimer, was carried out following established protocols [20]. For the synthesis of Ket-PEG4-N3, 2: A solution of norketamine (1.00 g, 3.85 mmol) in anhydrous DMF (12 mL) was reacted with NHS-PEG4-Azide (1.79g, 4.62 mmol). The mixture was stirred under nitrogen at room temperature overnight, with reaction progress monitored by TLC. The crude product was then diluted with DCM and washed three times with water (50 mL each). The organic layer was washed with brine, dried over sodium sulfate, and evaporated under vacuum to yield norketamine-PEG4-azide (1.82 g, 95%). Characterization by ^1H NMR (500 MHz,

DMSO-d6): 8.39 (singlet, Norketamine amine 1H), 7.35 (doublet, J = 6.5 Hz, Norketamine aromatic 1H), 7.30-7.20 (multiplet, Norketamine aromatic 3H), 3.85-3.08 (multiplet, Norketamine PEG H), 2.19-2.0 (multiplet, Norketamine 1H), 1.68-1.51 (multiplet, Norketamine 4H), 1.68-1.49 (multiplet, Norketamine 1H), and 1,27-1.10 (multiplet, Norketamine 2H).

Synthesis and characterization of GD-Ket involved stirring GD2-acetylene (300 mg, 0.02 mmol) with Norketamine-NHS-PEG4-azide (100 mg, 0.2 mmol) in a 1:1 DMF/H2O solution (5 mL). A catalytic amount of copper sulfate pentahydrate and sodium ascorbate was added, and the mixture was stirred at room temperature for 12 hours. It was then heated at 70 ºC under microwave conditions for 8 hours. The mixture was diluted with DMF, dialyzed against DMF for 12 hours (changing the solvent every 4 hours), followed by dialysis against water for another 12 hours (water changed every 2-3 hours). The final product was obtained by lyophilization as an off-white solid. 1H NMR (500 MHz, DMSO-d6) showed signals at 8.39 (s, 1H), 8.08-7.70 (m, 30H, triazole H), 7.51 (s, triazole H from Norketamine conjugation), 7.35 (d, J = 6.5 Hz, Norketamine aromatic H), 7.30-7.20 (m, Norketamine aromatic H), 5.07-4.04 (m, GD2 H), 4.14-4.12 (m, GD2 H), 3.66—3.08 (m, GD2 H and PEG H), 2.19-2.0 (m, Norketamine H), 1.90-1.60 (m, Norketamine H), 1.68-1.51 (m, Norketamine H), 1.68-1.49 (m, Norketamine H), 1,27-1.10 (m, Norketamine H).

In vitro release study of GD-Ket

An *in vitro* release study was conducted at plasma pH 7.4 and within the intracellular endosomal compartment at pH 5.5, with esterase in citrate buffer. GD-Ket solutions were prepared in PBS, and the citrate buffer with esterase was kept at 37ºC to simulate physiological conditions. Samples were collected periodically at designated time points. A standard curve for Ket was generated using HPLC at 260 nm. The released amount and percentage of Ket from GD-Ket were determined from the area under the curve, referencing the standard curve for free ketamine.

NMDAR functional assay

The NMDAR1A/2B antagonist activity of GD-Ket was evaluated by Eurofins DiscoverX using the SAFETYscan E/IC50 ELECT ion channel assay. Cells expressing the human NMDAR1A/2B ion channel were loaded with a fluorescent indicator dye and incubated with increasing concentrations of GD-Ket or free norketamine. Compounds were tested at 10 concentrations (1/3-diluted from the top concentration, 100 µM). Changes in ion channel activity were measured using a FLIPR Tetra® fluorescence plate reader, and concentration-response curves were generated to determine IC_{50} values by nonlinear regression. Detailed information on assay conditions is available at the Eurofins DiscoverX Corporation website.

Cell-based localization and efficacy studies

Cell culture: The HT-22 cells (Mouse Hippocampal Neuronal Cell Line, SCC129, Sigma-Aldrich) were cultured in expansion medium containing DMEM high-glucose medium (D7777, Sigma-Aldrich) with 10% heat-inactivated fetal bovine serum (FBS, A5256801, Gibco™) and 1% antibiotic-antimycotic solution (15240062, Gibco™) until 80% confluent [41]. Cultures were then incubated at 37°C in a CO_2 incubator with 5% CO2. The cells were then differentiated for 72 h in Neurobasal plus medium (A3582901, Gibco™) supplemented with 2 mmol of 1X L-glutamine (CAS Number: 56-85-9, Sigma-Aldrich) and 1X N2 supplement (17502048, Gibco™) as previously described [41].

Mitochondrial respiration assay using Seahorse XFe96 Analyzer: Mitochondrial respiration was assessed using an established advanced Seahorse technique using a Seahorse XFe96 analyzer (Agilent Technologies). HT-22 cells were grown [41] and plated at a density of 5,000 cells per well in a Seahorse XFe96 cell culture microplate the day prior to the experiment, except for the background-correction wells, which contained cell differentiation medium. The cells were

incubated in the cell culture incubator overnight. The Seahorse XFe96 utility plate and sensory cartridge were hydrated with Seahorse XF Calibrant (200 µL/well) for 24 h before the assay and incubated at 37°C in a non-CO2 incubator. On the day of the assay, the culture medium was replaced with Seahorse XF DMEM assay medium, supplemented with 1 mM pyruvate, 2 mM glutamine, and 10 mM glucose, pH 7.4. The plate was incubated at 37°C in a non-CO2 incubator for 1 hour before performing the assay. Mitostress assay reagents were prepared at 10x concentrations and loaded into the injection ports of the pre-hydrated Seahorse XFe96 sensor cartridge. Oligomycin (40 µM) was loaded into Port A, carbonyl cyanide-p-trifluoromethoxyphenylhydrazone (FCCP) (20 µM) into Port B, and a combination of rotenone (10 µM) and antimycin A (25 µM) into Port C.

To account for differences in cell numbers across wells, oxygen consumption rate (OCR) values from the mitochondrial stress test were normalized to nuclear staining. Immediately prior to the assay, NucBlue Live ReadyProbes Reagent (Hoechst 33342, R37605, Thermo Fisher Scientific, USA) was added to each well at a final concentration of 1 droplet per mL of assay medium. Plates were incubated for 30 min at 37 °C, protected from light, and then imaged using the Agilent BioTek Cytation 1. During image acquisition, the Agilent BioTek Cell Imaging software automatically segments Hoechst-positive nuclei and outputs the total number of nuclei per well. These cell count values are automatically transferred to the Wave software and used as the normalization parameter.

Mitochondrial Stress Test: The Mito stress test protocol began with three baseline measurements of oxygen consumption rate (OCR), alternating between 120 s of mixing and 120 s of measurement. Following baseline measurements, injections were made in the sequence of Port A (oligomycin), Port B (FCCP), and Port C (rotenone/antimycin A). For Ports A (oligomycin) and B (FCCP), five measurements were taken, alternating cycles of 120 s mixing, 60 s waiting, and 180 s measurement. For Port C (rotenone/antimycin A), eight measurements were taken with cycles of 120 s mixing, 60 s waiting, and 120 s measurement.

Mitochondrial bioenergetic parameters were calculated from the OCR measurements. Non-mitochondrial oxygen consumption (NMOC) was determined from the lowest OCR measured after the rotenone/antimycin A injection. Basal respiration was calculated as the OCR immediately before the first injection minus the NMOC. ATP production was derived by subtracting the last measurement before the oligomycin injection from basal respiration to the minimum rate after oligomycin injection. Maximal respiration was determined as the highest OCR following FCCP injection, minus the NMOC. Spare respiratory capacity was calculated as the ratio of maximal respiration to basal respiration, representing the cell's ability to respond to increased energy demand [42].

***In vitro* localization studies:** HT-22 cells were plated in 35-mm Ibidi dishes at a density of 5,000 cells per dish and differentiated as previously described. They were pre-treated with 100 μM glutamate for 4 hours, then incubated with 20 μg/ml of Cy5-labeled GD-Ket for 24 hours. Afterward, cells were treated again with 20 μg/ml Cy5-labeled GD-Ket for another 24 hours. Following the treatment, the cells were washed with PBS to remove excess compounds. For imaging, a Zeiss Confocal Microscope (model 710) was used. Images were acquired using differential interference contrast (DIC) and a Cy5 filter to detect the Cy5-labeled GD-Ket signal, and Z-stack imaging enabled precise spatial localization of the labeled compounds within the cells.

***In vitro* mechanistic studies:** HT-22 cells were seeded in 6-well plates (100,000 cells/well) and differentiated for 72 h as previously described[41]. We exposed the cells to 10 mM glutamate and treated them with vehicle, ketamine (10 μM), or GD-Ket (10 μM), with and without BD-1047 (3 nM; σ1-specific) [43]. At this concentration, BD-1047 exhibits high binding affinity for σ1 receptors with >50-fold selectivity over σ2 receptors. Testing at 3 nM yields effective fractional occupancy of σ1 near its binding affinity while remaining below the binding threshold for σ2. This concentration isolates the specific regulatory contribution of σ1 chaperone signaling at the

endoplasmic reticulum (ER)–mitochondrial membrane [43]. We removed Ket and GD-Ket after 4 h and incubated the cells overnight with glutamate and BD-1047. The following day, we collected the supernatants and then added 1X cell lysis buffer (Cell Signaling Technology; #9803) supplemented with 1X protease/phosphatase inhibitor cocktail (Cell Signaling Technology, #5872) and PMSF (Cell Signaling Technology; #8553). Cells were scraped from the bottom of the wells and incubated on ice for 30 min, followed by extraction and centrifugation at 14000 × g. The cell pellet was discarded, and lysates were collected for further analysis. The total protein content was measured using the BCA assay (Pierce™ BCA Protein Assay Kits, Thermo Fisher Scientific, USA). Subsequently, the levels of the cytokines, BDNF and NGF, were assessed using multiplex assays (U-PLEX Custom Metabolic Group 1 (ms) Assay Kits; Meso Scale Discovery; K152ACM-2).

Metabolite profiling and metabolic stability: The metabolic stability of Ket and GD-Ket was assessed using human liver microsomes, as previously described [44]. Stock solutions of Ket and GD-Ket were prepared at a concentration of 100 µM in 0.1 M potassium phosphate buffer (dPBS, pH 7.4). These stocks were then diluted to create a standard curve with concentrations of 1 µM, 0.1 µM, 0.01 µM, and 0.001 µM. For each test compound and control (negative and positive) 432 µL of pre-warmed PPBS, 50 µL of freshly prepared 10 mM NADPH, and 5 µL of the 100x test compound stock (final concentration of 1 µM) were added. The tubes were incubated for 5 min at 37°C. During this incubation, Human liver microsomes were thawed on ice and diluted to 20 mg protein/mL using PPBS. To initiate the reaction, 13 µL of the microsomes (final concentration of 0.5 mg/mL) was added to each tube, and the tubes were briefly vortexed. For the 0 min tubes, the reaction was immediately stopped by adding 250 µL of ice-cold acetonitrile, while for the 1hr/4hr tubes, the samples were incubated at 37°C for 1h / 4h before stopping the reaction with acetonitrile. After the reactions were stopped, the tubes were centrifuged at 10,000 g for 5 min at 4°C, and the supernatants were collected into HPLC vials. The samples were stored at -20 °C

until analysis. A standard curve was generated using the prepared dilutions, and the supernatants were analyzed by HPLC to determine the concentration of the parent compounds.

In vivo localization and efficacy assessments

Mice: All *in vivo* studies were performed in accordance with the protocol number MO21M208, which received approval on August 8, 2021, from the Johns Hopkins University Animal Care and Use Committee (IACUC). ARRIVE guidelines 2.0 were followed for all *in vivo* experiments [45]. 6–8-week-old male wild-type C57BL/6 mice (Jackson Laboratory, RRID: IMSR_JAX:000664) were used for the efficacy studies. Since male mice are more susceptible to severe pilocarpine-induced seizures and the development of SE, including neuronal death, glial activation, and inflammatory changes post-seizures [46] [47], detailed dose optimization studies followed by efficacy were evaluated in the more severe male phenotype. In rodents, estrogen and progesterone have been shown to reduce seizure severity and protect against the development of SE [46,48]. Moreover, population studies have shown an increased incidence of SE in males [49]; therefore, our main study included a larger cohort of male mice. Considering sex as a biological variable, a separate cohort of female mice (n = 7-9/group) was used to conduct acute SE studies in females **(Fig S6),** as carried out in male mice.

For biodistribution studies, Thy-1 YFP (strain #003709) mice were used (Jackson). The animals were housed and maintained in the animal facility at 25 ºC under a 12 h light-dark cycle (food and water *ad libitum*). Animals were closely monitored for post-pilocarpine-induced seizures and for signs of pain and suffering and euthanized as per protocol.

Experimental paradigm: All treatments (GD-Ket, Ket, and saline-vehicle solutions) were prepared as sterile single doses and were administered to the mice in a blind manner. A computer-generated randomization scheme was used to randomize the mice to the five treatment groups: (1) WT, (2) Pilocarpine (Pilo/Sal; 280 mg/kg), (3) Pilocarpine + GD-Ket (Pilo/GD-Ket, 0.3 mg/Kg

IP on ketamine basis), or (4) Ket (Pilo/Ket, 0.3 mg/Kg IP) dissolved in saline, accounting for higher mortality in the untreated groups. Animals were numbered and assigned to treatment groups. An initial dose-response study was done with 0.3, 3, and 30 mg/kg of GD-Ket to determine the lowest effective dose. A separate cohort of mice exposed to pilocarpine was tested with GD alone at the equivalent dose and showed no efficacy. Subsequently, all studies were done in comparison to saline vehicles.

***In vivo* imaging of healthy and pilocarpine-induced C57Bl/6 mice:** A biodistribution study was conducted to evaluate the *in vivo* distribution of Cy5-GD-Ket in healthy and pilocarpine-induced mice. Cy5-GD-Ket was administered *via* the intraperitoneal route, and whole-body imaging was performed at multiple time points (3, 6, 12, 24, 48, and 72 h) post-injection. Mice were anesthetized with isoflurane, and fluorescence distribution was monitored over time using a near-infrared fluorescence imaging system (PerkinElmer IVIS Spectrum BL) with autoexposure and a band-pass filter (λ_{ex}: 620 ± 20 nm / λ_{em}: 670 ± 20 nm). At 72 h, all organs, including the brain, were collected. Brains were micro-dissected into the hippocampus, cortex, cerebellum, thalamus, striatum, and brainstem. The fluorescence signals from each region were captured for region-specific further analysis.

***In vivo* localization studies:** In separate cohorts of healthy and pilocarpine-induced animals, the biodistribution of GD and GD-Ket conjugated with the Cy5 fluorophore was investigated. The Cy5-labeled GD-Ket (Cy5-GD-Ket) was administered intraperitoneally (0.3 mg/kg) 15min after administration of the intraperitoneal pilocarpine injection of 280 mg/kg. Mice dosed with GD-Cy5 were perfused and fixed after 4 h; brains were collected to assess Cy5-GD-Ket localization.

Cy5-GD-Ket extraction and fluorescence quantification (*ex vivo* biodistribution studies): Tissue samples were processed for biodistribution by homogenization and extraction using established methods. All organs were harvested, frozen on dry ice, and stored at- 80 °C until ready for processing. Blood was collected in heparin-coated tubes (Sigma), centrifuged, and the plasma supernatant was removed and stored in protein lo-bind Eppendorf tubes (Sigma) at- 80°C.

The organs were later thawed, weighed, and dissected. These tissues were homogenized in methanol at a ratio of 1 ml per 100 mg of tissue, using 0.9–2.0 mm stainless steel beads on a Bullet Blender Storm 24 tissue homogenizer (Next Advantage Inc., Averill Park, NY) for 10 minutes at power level 6 for brain and spleen, and level 12 for liver, lungs, and kidneys. Following homogenization, samples were centrifuged at 15000 rpm for 10 minutes at 4°C. The supernatant was transferred to protein lo-bind Eppendorf tubes and stored at- 80°C. Plasma samples were diluted tenfold in dPBS and filtered through a 0.2 µm PES filter. Prior to fluorescence measurement, HPLC analysis of supernatants confirmed the stability of the conjugates *in vivo*. Fluorescence intensity of Cy5 (excitation at 645 nm, emission at 662 nm) was measured with a RF6000 Spectrofluorophotometer using Lab Solutions RF software (Shimadzu), with background fluorescence adjustments based on healthy control tissue. The fluorescence intensity values were then converted to dendrimer concentration using batch-specific calibration curves for Cy5-GD-Ket, following unblinding of sample identifications.

Pilocarpine-induced convulsive SE: The efficacy of GD-Ket was investigated in the chemically induced pilocarpine model of convulsive SE. This model mimics several characteristic clinical features of RSE, including the development of localized lesions in the CA1, CA3, and DG regions and mossy fiber sprouting post-SE [26]. The 6-8-week-old C57Bl/6 male mice received scopolamine (2mg/kg IP) 30 min before pilocarpine injection (280 mg/kg IP). Once the establishment of SE (at least stage 4 or higher on the Racine scale [28,33] for 5 min or more) was confirmed, we administered the therapy. During this time, stage 3–5 seizures typically range from 15 to 90 s, with periods of relative inactivity or other variable stages in between. We counted generalized seizures as seizures that involved the whole body, including whole-body clonus, loss of limb control, generalized tonic-clonic seizures, episodes of rearing, and loss of balance **(Table S2)**. Some animals also experienced rearing episodes, generalized tonic extension of the body, and cardiopulmonary collapse, leading to death. We counted and scored the first 120 min post-therapy administration; however, we continuously observed the animals for survival post-seizure

termination for 3-5 h, followed by occasional checks to calculate survival rates until euthanasia. We supplemented surviving animals with lactated Ringer's solution, transferred them to cages, and returned them to the vivarium once actively moving around. Behavioral scoring using the Racine scale shows a reduction in behavioral seizures, and we do not confirm electrographic seizure termination.

Post SE care: Mice that continued to experience stage 4-6 seizures beyond the observation period (after ~120 min) were treated with diazepam (10 mg/kg IP) on ethical grounds to terminate the seizures. Once the behavioral seizures subsided, we returned the mice to their home cages and monitored them 2-3 times daily till euthanized. We conducted daily assessments for regular activity and signs of distress multiple times a day. The animals received softened food and hydrogel in the cage. Whenever needed, we hydrated them with sterile Ringer's lactate injections after they were returned to the home cages.

Quantitative video electroencephalography (vEEG) recordings: Continuous video-EEG monitoring was done using the Pinnacle hardware and the Sirenia® Acquisition software suite. Male mice (N = 3 per group) were surgically implanted with a prefabricated 2 EEG/1 EMG head mount (8201-SS, Pinnacle Technology Inc., Lawrence, KS, USA). Animals were anesthetized with isoflurane and secured in a stereotaxic frame. After exposing and cleaning the cranium, pilot holes were drilled through the skull, and 0.10" and 0.12" stainless-steel screws (8209 and 8212, Pinnacle Technologies, USA), serving as cortical recording electrodes, were secured into the subdural space without disrupting the underlying brain parenchyma. The prefabricated 2 EEG/1 EMG head mount was aligned over the skull and positioned relative to the bregma. Conductive silver epoxy (8226: Silver Epoxy, Pinnacle Technologies, USA) was used to establish electrical contact between the head mount leads and the cortical screws. Flexible EMG wire leads were inserted into the nuchal muscles to monitor muscle tone and artifacts. The head mounts and exposed skull were then secured and sealed with dental cement.

Animals received postoperative analgesia and were allowed to recover for 7 days before SE induction. Subsequently, the head mount was connected to the preamplifier, which was connected to the recording system and its power supply (±4.5 V), as well as to the differential AC amplifier inputs. We used a high-pass filter at 0.1 Hz and a low-pass filter at 1 kHz. We set the overall gain of the preamplifier and amplifier to 100X and determined that a sampling rate of 2000 Hz was sufficient to provide sufficient resolution for high-frequency tracking during severe seizures. SE termination was defined as sustained suppression of these high-amplitude seizure clusters, increased interictal intervals, and a return toward the power spectral density.

For each recording session, mice were transferred to the EEG room and habituated to the chamber 30 min before recording. Baseline EEG was recorded before pilocarpine administration to establish resting activity using the 3-chamber EEG system (Pinnacle Technologies, USA). After seizure induction, continuous recordings were obtained to monitor the evolution of ictal activity and to evaluate treatment-induced SE termination. Signal processing and power spectral analysis were performed using Sirenia® Seizure Pro software (version 3.3.2) to quantify total signal power across major frequency bands before and after treatment.

Long-term behavior

Open-field test: At 4 months post-SE, exploratory and locomotor behaviors were assessed in an open-field (40 × 40 × 40 cm). Mice were habituated to the testing room for 60 minutes, then individually placed in the center and observed for 10 min. Video-tracking software (AnyMaze, version 7.67) recorded the total distance traveled, mean speed, and time spent in the center to periphery zones. The arena was cleaned with 70% ethanol between trials. [30].

Rotarod test: Motor coordination and learning were assessed 4 months post-SE using an accelerating Rotarod system (Columbus Instruments, USA) with Rotamex-5 software version 1.3.2. Mice were first habituated to a stationary rod and then to a constant speed of 4 rpm. Subsequently, animals underwent 3 accelerating trials per day, starting at 4-40 rpm for 5 min.

Latency to fall was recorded automatically to evaluate long-term motor performance and learning acquisition [50].

Tissue Processing, Immunohistochemistry and Imaging

Tissue processing: Brains were harvested and quickly micro-dissected for biochemical analysis; brain regions were flash-frozen in liquid nitrogen 48 h after injury. Protein samples, normalized in concentration, were added to the respective MSD (V-PLEX Proinflammatory Panel 1 Mouse Kit, K15048D, Meso Scale Discovery, USA) or pre-coated ELISA plates. Plates were incubated and processed according to the manufacturer's instructions.

For histopathological analysis, brain samples to evaluate biodistribution were collected 4 h after dendrimer administration, while samples for efficacy were obtained 48 h post-SE. Animals were deeply anesthetized with 2-4% isoflurane, transcardially perfused with at least 60 mL of PBS (pH 7.4), then with 10% NBF, and post-fixed overnight. Biodistribution samples were perfused only with PBS and post-fixed in 10% NBF overnight. Brains were cryoprotected with 30% sucrose until sinking, then sectioned into 30 µm coronal slices using a sliding microtome (RM2125 RTS, Leica Biosystems, Nussloch, Germany) for efficacy or a cryostat for biodistribution, mounted on slides, and stored at -20 °C in antifreeze media or on slides until further processing.

Immunohistochemistry: For efficacy assessment, free floating brain sections were rinsed from antifreeze medium in 1x TBS for 10 min, incubated in 0.05% $NaBH_4$ in dH_2O (Sigma Aldrich, 452882, MO, USA) for 10 min, and washed 3 times in 1x TBS for 10 min followed by incubation for 1.5 h at room temperature in a blocking solution containing 0.25%TritonX-100/TBS (80%), Normal Donkey Serum (10%,) and 3% BSA/PBS (10%) and then incubated in rabbit anti-Iba-1 (1:250, 019-19741, Wako, Japan) primary antibody overnight at 4ºC. Sections were then washed 3 times in 1x TBS for 10 min and incubated in Alexa Fluor 594 Donkey anti-rabbit IgG (1:1000, A21207, Invitrogen, USA) as a secondary antibody for 1.5 h. Tissue was washed 3 times in 1x

TBS and incubated in DAPI (1:1000) for 10 min, quickly rinsed in 1x TBS, mounted on microscope slides, allowed to airdry and coverslipped with ProLong Gold antifade reagent. For biodistribution assessment with Iba-1 for microglia, brain sections were stained on the slides as above, with the following differences: no NaBH4 was used, and the blocking solution used was 0.1% TritonX-100/TBS instead of 0.25%. For biodistribution assessment with Thy-1, tissue was rehydrated for 10 min in 1x TBS, incubated with DAPI (1:1000) in 1x TBS for 10 min, rinsed with 1x TBS, air-dried, and coverslipped with ProLong Gold antifade reagent.

Imaging: Biodistribution and co-localization imaging were done using confocal imaging on a Leica SP8 microscope; low-magnification images were taken with a 20x objective (HC PL APO CS2 20x/0.75 DRY) and high-magnification images with a 63X objective (HC PL APO CS2 63x/1.40 OIL). For co-localization of dendrimers in neurons, a Z-stack (16 steps of 2 µm each) was acquired; 63x images are shown as a maximum projection. To confirm co-localization, an orthogonal section was taken on an enlarged image from the 63x-magnified Z-stack. Efficacy assessment of neuroprotection and neuroinflammation was performed using fluorescence imaging on a Leica DM6B-Z microscope and a Leica-K8-A24G726030 camera; images were taken with a 10X objective (HC PL FLUOTAR 10x/0.32 DRY). Microglia outlines were captured with a 20x objective (HC PL APO 20x/0.80 DRY), and Lightning deconvolution and outline generation were performed following published methods with minor modifications [51]. Briefly, images were post-processed in Fiji, converted to 8-bit grayscale, and brightness/contrast adjusted to the histogram. An unsharp mask filter was applied, and noise reduction was performed using the despeckle function; images were then converted to binary through thresholding (default setting), and a second round of despeckle noise reduction was performed, connecting closed dark pixels with the close function and removing outliers.

Respiratory depression studies and determination of composite sedation scores

We treated adult, 10-week-old C57BL/6 WT mice with increasing doses of ketamine (75, 100, 200, or 300 mg/kg IP) or GD-Ket (100, 200, or 300 mg/kg IP) and observed them in an open field for 660 min to evaluate acute effects. *Activity post-administration* was analyzed for total distance traveled using automated analysis with *AnyMaze version 7.67*. Composite sedation scores were determined manually by a blinded experimenter using a modification of the Minho Objective Rodent Phenotypical Anesthesia (MORPhA) scale[52] and Respiratory Distress Observation Scale for patients [53] **(Table S3)**. Our modified scale included Ataxia (0-3), mobility and gait (0-5), and respiration (0-5). For each mouse, the highest scores for ataxia, mobility and gait, and respiration were added to determine the composite sedation score. We used aggregated scores for comparisons, with 0 corresponding to normal function, and higher scores indicating a progressively greater degree of sedation, culminating in death [53].

Statistics

All data analyses were performed using GraphPad Prism software (version10.4.1, Boston, MA, USA). Statistical significance was considered at $p < 0.05$, and all tests were two-sided.

In vitro studies:

Unless otherwise stated, all the *in vitro* data were analyzed using mean values ± SD. Group comparisons were made using t-tests, one-way or Two-way ANOVA, followed by multiple comparison tests.

In vivo studies:

Long-term behavioral and seizure observations: For our *in vivo* studies, we determined sample size based on pilot experiments conducted in our lab under similar conditions to the main trials. Using G*Power (version 3.1.9 for Mac OS), we performed an a priori power analysis with α set at 0.05, a power (1-β) of 0.95, and an allocation ratio (n1/n2) of 1. The estimated effect size was 1.95, resulting in a calculated sample size of 8 per group. Because Pilo/Sal groups may have

higher mortality, some adjustments might be needed [25]. We expected some animals might not survive until the 48-hour mark. Consequently, we randomly assigned animals to groups of different sizes and kept the experimenters blinded during behavioral tests. Survival rates in mice were analyzed with Fisher's exact test, while seizure durations over time were evaluated using repeated-measures ANOVA. Unless specified otherwise, all statistical comparisons used Tukey-Kramer's method. Data analysis was performed with GraphPad Prism (version 10.4.1), considering $p < 0.05$ as significant for two-sided tests.

For EEG analysis, we applied Fast Fourier Transform (FFT) power spectral analysis to the EEG signals using Sirenia Seizure Pro software version 3.1.2 (Pinnacle Technologies, USA). A Hanning window was used to reduce spectral leakage. Similar to behavioral data, repeated-measures ANOVA assessed power changes over time, with Tukey-Kramer's multiple comparisons unless noted otherwise. Data were analyzed using GraphPad Prism software (version 10.4.1), with significance set at $p<0.05$ for two-sided tests.

Discussion

In this study, we report a novel GD-Ket conjugate in which our neuron-targeting glucose dendrimer is conjugated to ~7 molecules of norketamine using a stable, relatively non-cleavable amide bond. Based on the functional assay and the release profile, we show that GD-Ket is active in the conjugated form. Our study shows that GD-Ket is effective at doses ~30-80 times lower than those typically reported for ketamine in this model [17,54] in reducing seizures, improving survival, and decreasing neuronal death and neuroinflammation. We showed that GD-Ket exhibits significant efficacy even when administered to animals with pre-existing seizure circuits, unlike previous preclinical studies in which anti-seizure medications were administered as preventive therapies. Treatments administered after the establishment of seizure circuits often fail to effectively manage neurological emergencies such as RSE or SRSE [55]. The efficacy of GD-Ket in a model of ***established SE*** preserves the clinical and translational relevance. These efficacies seem to be due not only to its action on NMDARs but also to its intracellular action through

modulation of chaperone protein receptors. Modulation of σ chaperone receptors has shown potential for controlling seizures preclinically [56,57]. Both activation and inhibition of σ chaperone protein receptors have shown neuroprotective properties; depending on the context and disease, their cellular signaling effects are not solely determined by simple activation or blockade, but rather by their role as a molecular chaperone that engages with numerous proteins within a specific cellular and physiological environment based on the diseased state [58].

Importantly, unlike free ketamine, we show that GD-Ket is metabolically stable without the formation of active metabolites by the liver and safely delivers the drug to areas involved in seizures without debilitating off-target effects. We also showed that although GD-Ket localizes intracellularly, unlike free ketamine, it does not lead to mitochondrial toxicity. The *in vivo* safety observed even at 1000x the therapeutic dose is likely due to the specific localization and targeting of GD-Ket, primarily in actively seizing neurons and glia in brain regions associated with RSE and super-refractory SE (SRSE), without any CNS or systemic side effects. We expect that GD-Ket, which is not taken up by injured neurons and glia, will be excreted intact in urine, as previously described for dendrimer platforms [59]. These data indicate a wide therapeutic window for GD-Ket, highlighting the potential of safely administering this drug in the field and in outpatient settings or hospitals to rapidly arrest convulsive SE.

Ketamine has gained interest as a third-line agent for RSE and SRSE. Ketamine shows variable efficacy at a dose range of 1.2 to 15 mg/kg/h via IV infusion in RSE patients, has been administered for up to 287 days [7], and has been associated with high relapse rates after discontinuation [60]. Safety concerns with ketamine include respiratory depression, metabolic acidosis, and hemodynamic instability with long-term infusions, particularly in critically seizing patients, limiting its use as a first-line agent[60]. While intranasal spray of (S)-ketamine (esketamine) is approved by the US FDA for treatment-resistant depression, it requires medical supervision due to risks of abuse, sedation, fatal respiratory depression, and dissociation [61].

Ketamine at sub-anesthetic doses has demonstrated efficacy in chronic pain management, in treatment-resistant depression, bipolar disorders, schizophrenia, and substance use disorders, and is being explored for neurodevelopmental disorders such as Rett syndrome [3,10,61]. These broad efficacies are attributed to its unique pharmacological profile, which involves modulation of NMDARs, opioid receptors, σ receptors, and monoamines, positioning it for potential applications in several neuroinflammatory and neurological disorders [16]. GD-Ket enhances the efficacy of ketamine in a targeted manner without the safety concerns and by uncoupling its anesthetic effects from its other therapeutic targets.

Recent literature highlighting innovative drug delivery strategies for neurological disorders, particularly epilepsy, underscores the growing clinical need for targeted therapeutic systems[62–64]. Several ketamine nanoformulations, such as ketamine-encapsulated PLGA [65], PEG-PLGA nanoparticles [66], ultrasound-activated nanoparticles [67], and multifunctional nanocarrier systems [68], have been tested to address these limitations. The glucose dendrimer platform enables targeted intracellular delivery to affected brain regions, thereby preventing off-target effects. Since patients with neurological disorders such as RSE require rapid, efficient delivery to specific brain areas [63], GD-Ket nanotherapy holds significant promise. Our data show that GD-Ket successfully addresses the typical challenges associated with ketamine nano formulations, including the complexities of ketamine conjugation and scale-up synthesis, the necessity of additional ligands or stimuli for targeted delivery, potential systemic toxicity arising from unpredictable release profiles, the absence of an established *in vivo* efficacy profile, and uncertainty surrounding long-term safety [18,19].

Our data indicate that GD is a powerful platform for delivering drugs primarily to specific neuronal subsets. This may also avoid the psychomimetic or hallucinogenic potential of free ketamine. Our hydroxyl PAMAM dendrimer conjugate (OP-101®) has previously shown significant benefits in severe COVID-19 patients in the ICU through Phase 2 trials, decreasing cytokine levels and

hyperinflammation, improving survival, and potentially addressing the neurological consequences of COVID-19 by crossing the blood-brain barrier [18]. The lack of liver toxicity and liver metabolism has been clinically demonstrated for the dendrimer platform, in which a dendrimer-sunitinib analog conjugate (D-4517.2®) showed promising efficacy in Phase 2 trials for the systemic treatment of wet age-related macular degeneration and diabetic macular edema, with no adverse effects even with chronic dosing [19].

GD-Ket therapy has potential for clinical translation for SE, enabling safe administration outside the ICU setting for rapid and early control of refractory seizures, including conditions like new-onset refractory *status epilepticus* (NORSE), which can have devastating long-term consequences due to widespread neuronal injury. The safety and broad therapeutic index of GD-Ket would enable its development for use in the field or in emergency and acute care settings. This study did not investigate the efficacy of GD-Ket in preventing spontaneous recurrent seizures as seen in temporal lobe epilepsy, which could provide long-term benefits for patients with temporal lobe epilepsy. These will be addressed in future studies.

4. Conclusion

In this study, we demonstrate that GD-Ket is a potent, safe, and clinically translatable nanotherapeutic platform that fundamentally redefines the utility of ketamine for life-threatening seizure emergencies. By conjugating norketamine to a neuron-targeted glucose dendrimer through a stable amide bond, GD-Ket achieves selective uptake into metabolically stressed neurons and microglia in seizure-involved brain regions, while avoiding off-target CNS effects and hepatic metabolism. At doses 30–80x lower than typical ketamine requirements, GD-Ket robustly reduced seizure burden, improved survival, and attenuated hippocampal neurodegeneration, neuroinflammation, and long-term behavioral outcomes in an established model of convulsive SE. Importantly, GD-Ket exhibited no sedation, respiratory depression, or toxicity even at 1,000× the efficacious dose, highlighting an exceptional therapeutic window not achievable with free

ketamine. Mechanistically, GD-Ket not only preserves and enhances ketamine's NMDA receptor antagonism through multivalency but also exerts intracellular actions through modulation of σ chaperone receptors, likely via allosteric interaction. This dual mechanism contributes to its broad neuroprotective and anti-inflammatory efficacy while uncoupling ketamine's therapeutic benefits from its anesthetic and psychomimetic liabilities.

In summary, GD-Ket is a compelling, clinically actionable dendrimer-based nanotherapy that harnesses ketamine's neurotherapeutic potential while overcoming its long-standing safety limitations. Its targeted action and wide safety margin support the safe deployment of ketamine-based therapy in emergency, pre-hospital, and acute care settings, enabling rapid control of refractory and life-threatening seizures, including RSE and NORSE. Together, these findings position GD-Ket as a first-in-class, neuron-targeted therapeutic with strong potential for clinical translation in status epilepticus and other severe neurological disorders.

Availability of data and materials: Data will be made available on request.

Acknowledgments: All schematics used in this manuscript were created in BioRender.com.

Funding Statement: This work was supported in part by Samata Therapeutics, Inc. (SK, RMK) through a joint research agreement with Johns Hopkins and the National Institutes of Health, DHHS, NINDS Grant R01NS931204 (RMK, SK).

Author contributions:

Preeti Vyas: Writing, Review & editing, Validation, Data Curation, Conceptualization
Wathsala Liyanage: Writing, Review & editing, Validation, Data curation, Conceptualization
Javier Allende Labastida: Data Curation, Validation
James L. Sowers: Data Curation, Validation
Milan Paul: Data Curation, Validation
Kavichandhirakanth Murugesan: Data Curation, Validation
Bruno Henrique Dallo Gallo: Data Curation, Validation
Susanna Scafidi: Data Curation, Validation
Kathleen Lac: Data Curation
Lirong Shao: Data Curation, Validation, Review & editing
Narendra Kale: Data Curation
Maria Paula Avalos: Data Curation
Carl E. Stafstrom: Validation, Review & editing
Kunal S. Parikh: Writing, Review & editing, Validation, Conceptualization, Resources

Rangaramanujam M. Kannan: Writing, Review & editing, Validation, Conceptualization, Resources
Sujatha Kannan: Writing, Review & editing, Validation, Conceptualization, Resources

Conflicts of Interest: Under license agreements involving Samata Therapeutics and Johns Hopkins University, RMK, SK, KSP, and the University are entitled to royalty distributions and share ownership/equity related to the dendrimer-ketamine conjugate discussed in the manuscript. RMK, SK and KSP are co-founders of Samata Therapeutics. WL and PV are part of the IP related to this compound and are entitled to royalties. This work was funded in part by Samata Therapeutics through a joint research agreement with Johns Hopkins University.

References

1. Orser BA, Pennefather PS, MacDonald JF. Multiple Mechanisms of Ketamine Blockade of N-methyl-D-aspartate Receptors. Anesthesiology [Internet]. 1997 [cited 23 September 2025]; 86: 903–17. Available at: https://journals.lww.com/00000542-199704000-00021

2. Zanos P, Gould TD. Mechanisms of ketamine action as an antidepressant. Mol Psychiatry. 2018; 23: 801–11.

3. Nowacka A, Borczyk M. Ketamine applications beyond anesthesia - A literature review. Eur J Pharmacol. 2019; 860: 172547.

4. Hess EM, Riggs LM, Michaelides M, Gould TD. Mechanisms of Ketamine and its Metabolites as Antidepressants. Biochem Pharmacol. 2022; 197: 114892.

5. Williams NR, Heifets BD, Blasey C, et al. Attenuation of Antidepressant Effects of Ketamine by Opioid Receptor Antagonism. Am J Psychiatry. 2018; 175: 1205–15.

6. Ma H, Li J-F, Qiao X, et al. Sigma-1 receptor activation mediates the sustained antidepressant effect of ketamine in mice via increasing BDNF levels. Acta Pharmacol Sin. 2023;

7. Alkhachroum A, Der-Nigoghossian CA, Mathews E, et al. Ketamine to treat super-refractory status epilepticus. Neurology. 2020; 95: e2286–94.

8. Balzer N, McLeod SL, Walsh C, Grewal K. Low-dose Ketamine For Acute Pain Control in the Emergency Department: A Systematic Review and Meta-analysis. Acad Emerg Med Off J Soc Acad Emerg Med. 2021; 28: 444–54.

9. Glue P, Neehoff S, Beaglehole B, Shadli S, McNaughton N, Hughes-Medlicott NJ. Ketamine for treatment-resistant major depressive disorder: Double-blind active-controlled crossover study. J Psychopharmacol Oxf Engl. 2024; 38: 162–7.

10. Campbell K, Neul JL, Lieberman DN, et al. A randomized, placebo-controlled, cross-over trial of ketamine in Rett syndrome. J Neurodev Disord [Internet]. 2025 [cited 4 September 2025]; 17: 4. Available at: https://jneurodevdisorders.biomedcentral.com/articles/10.1186/s11689-025-09591-y

11. Orhurhu VJ, Vashisht R, Claus LE, Cohen SP. Ketamine Toxicity. In: StatPearls [Internet]. Treasure Island (FL): StatPearls Publishing; 2024 [cited 18 March 2024]. Available at: http://www.ncbi.nlm.nih.gov/books/NBK541087/

12. Schep LJ, Slaughter RJ, Watts M, Mackenzie E, Gee P. The clinical toxicology of ketamine. Clin Toxicol Phila Pa. 2023; 61: 415–28.

13. Strous JFM, Weeland CJ, van der Draai FA, et al. Brain Changes Associated With Long-Term Ketamine Abuse, A Systematic Review. Front Neuroanat. 2022; 16: 795231.

14. Trinka E, Cock H, Hesdorffer D, et al. A definition and classification of status epilepticus – Report of the ILAE Task Force on Classification of Status Epilepticus. Epilepsia [Internet]. 2015 [cited 28 May 2025]; 56: 1515–23. Available at: https://onlinelibrary.wiley.com/doi/10.1111/epi.13121

15. Rossetti AO, Lowenstein DH. Management of refractory status epilepticus in adults: still more questions than answers. Lancet Neurol [Internet]. 2011 [cited 13 October 2025]; 10: 922–30. Available at: https://linkinghub.elsevier.com/retrieve/pii/S1474442211701879

16. Zorumski CF, Izumi Y, Mennerick S. Ketamine: NMDA Receptors and Beyond. J Neurosci [Internet]. 2016 [cited 25 September 2025]; 36: 11158–64. Available at: https://www.jneurosci.org/lookup/doi/10.1523/JNEUROSCI.1547-16.2016

17. Tannich F, Hamlaoui S, Hamdi Y, Souilem O. Ketamine Protects Against Pilocarpine-Induced Oxidative Stress and Metabolic Enzyme Disturbances During Epileptogenesis in the Epilepsy Model. Pharm Chem J [Internet]. 2024 [cited 14 June 2025]; 58: 1029–38. Available at: https://link.springer.com/10.1007/s11094-024-03239-2

18. Gusdon AM, Faraday N, Aita JS, et al. Dendrimer nanotherapy for severe COVID-19 attenuates inflammation and neurological injury markers and improves outcomes in a phase2a clinical trial. Sci Transl Med [Internet]. 2022 [cited 17 March 2025]; 14: eabo2652. Available at: https://www.science.org/doi/10.1126/scitranslmed.abo2652

19. Ashvattha Therapeutics Presents Positive Interim Phase 2 Results for Subcutaneous Migaldendranib Treatment for DME and Wet-AMD at 2025 MaculArt Meeting [Internet]. 2025. Available at: https://avttx.com/ashvattha-therapeutics-presents-positive-interim-phase-2-results-for-subcutaneous-migaldendranib-treatment-for-dme-and-wet-amd-at-2025-maculart-meeting/

20. Sharma A, Sah N, Sharma R, et al. Development of a novel glucose-dendrimer based therapeutic targeting hyperexcitable neurons in neurological disorders. Bioeng Transl Med [Internet]. 2024 [cited 28 May 2025]; 9: e10655. Available at: https://aiche.onlinelibrary.wiley.com/doi/10.1002/btm2.10655

21. Zhang W, Dhumal D, Zhu X, et al. Bola-Amphiphilic Glycodendrimers: New Carbohydrate-Mimicking Scaffolds to Target Carbohydrate-Binding Proteins. Chem – Eur J [Internet]. 2022 [cited 14 December 2025]; 28: e202201400. Available at: https://chemistry-europe.onlinelibrary.wiley.com/doi/10.1002/chem.202201400

22. Bian Z, Zhang W, Garofalo S, et al. Bola-amphiphilic glycodendrimers for targeting glial cells in the brain. Nanoscale [Internet]. 2025 [cited 14 December 2025]; 17: 27869–80. Available at: https://xlink.rsc.org/?DOI=D5NR03017J

23. Liyanage W, Vyas P, Kale N, et al. Glucose dendrimer-ketamine conjugates enable precise and efficacious neuromodulation while preserving neuronal network dynamics. Nano Today [Internet]. 2027 [cited 7 October 2026]; 72: 103193. Available at: https://linkinghub.elsevier.com/retrieve/pii/S1748013226002215

24. Giuliano K, Etchill E, Zhou X, et al. NMDA Receptor Antagonism for Neuroprotection in a Canine Model of Hypothermic Circulatory Arrest. J Surg Res [Internet]. 2021 [cited 23 July 2026]; 260: 177–89. Available at: https://linkinghub.elsevier.com/retrieve/pii/S0022480420308349

25. Choi SK, Thomas TP, Li M-H, Desai A, Kotlyar A, Baker JR. Photochemical release of methotrexate from folate receptor-targeting PAMAM dendrimer nanoconjugate. Photochem Photobiol Sci [Internet]. 2012 [cited 23 July 2026]; 11: 653–60. Available at: https://link.springer.com/10.1039/c2pp05355a

26. Shibley H, Smith BN. Pilocarpine-induced status epilepticus results in mossy fiber sprouting and spontaneous seizures in C57BL/6 and CD-1 mice. Epilepsy Res [Internet]. 2002 [cited 14 June 2025]; 49: 109–20. Available at: https://linkinghub.elsevier.com/retrieve/pii/S0920121102000128

27. Kolasa K, Kleinrok Z, Consolo S, Ferrario P, Zecca L. Susceptibility to seizures produced by chemical convulsants and maximal electric shock in rats after electrolytic lesions into the red nucleus. Pharmacol Biochem Behav [Internet]. 1992 [cited 14 June 2025]; 41: 99–103. Available at: https://linkinghub.elsevier.com/retrieve/pii/009130579290066O

28. Racine RJ. Modification of seizure activity by electrical stimulation: II. Motor seizure. Electroencephalogr Clin Neurophysiol [Internet]. 1972 [cited 14 June 2025]; 32: 281–94. Available at: https://linkinghub.elsevier.com/retrieve/pii/0013469472901770

29. Blair RE, Deshpande LS, Holbert WH, Churn SB, DeLorenzo RJ. Age-dependent mortality in the pilocarpine model of status epilepticus. Neurosci Lett [Internet]. 2009 [cited 28 January 2026]; 453: 233–7. Available at: https://linkinghub.elsevier.com/retrieve/pii/S0304394009002171

30. Curia G, Longo D, Biagini G, Jones RSG, Avoli M. The pilocarpine model of temporal lobe epilepsy. J Neurosci Methods [Internet]. 2008 [cited 28 January 2026]; 172: 143–57. Available at: https://linkinghub.elsevier.com/retrieve/pii/S0165027008002550

31. Covolan L, Mello LEAM. Temporal profile of neuronal injury following pilocarpine or kainic acid-induced status epilepticus. Epilepsy Res [Internet]. 2000 [cited 28 January 2026]; 39: 133–52. Available at: https://linkinghub.elsevier.com/retrieve/pii/S0920121199001199

32. Fabene PF, Merigo F, Galiè M, et al. Pilocarpine-Induced Status Epilepticus in Rats Involves Ischemic and Excitotoxic Mechanisms. Akbarian S, Ed. PLoS ONE [Internet]. 2007 [cited 28 January 2026]; 2: e1105. Available at: https://dx.plos.org/10.1371/journal.pone.0001105

33. Borges K. Neuronal and glial pathological changes during epileptogenesis in the mouse pilocarpine model. Exp Neurol [Internet]. 2003 [cited 14 June 2025]; 182: 21–34. Available at: https://linkinghub.elsevier.com/retrieve/pii/S0014488603000864

34. Oliveira CVD, Grigoletto J, Funck VR, et al. Evaluation of potential gender-related differences in behavioral and cognitive alterations following pilocarpine-induced status epilepticus in C57BL/6 mice. Physiol Behav [Internet]. 2015 [cited 25 July 2026]; 143: 142–50. Available at: https://linkinghub.elsevier.com/retrieve/pii/S0031938415001304

35. Vezzani A, French J, Bartfai T, Baram TZ. The role of inflammation in epilepsy. Nat Rev Neurol [Internet]. 2011 [cited 14 June 2025]; 7: 31–40. Available at: https://www.nature.com/articles/nrneurol.2010.178

36. Benson MJ, Manzanero S, Borges K. Complex alterations in microglial M1/M2 markers during the development of epilepsy in two mouse models. Epilepsia [Internet]. 2015 [cited 14 June 2025]; 56: 895–905. Available at: https://onlinelibrary.wiley.com/doi/10.1111/epi.12960

37. Vezzani A, Di Sapia R, Kebede V, Balosso S, Ravizza T. Neuroimmunology of status epilepticus. Epilepsy Behav [Internet]. 2023 [cited 28 May 2025]; 140: 109095. Available at: https://linkinghub.elsevier.com/retrieve/pii/S1525505023000136

38. Ma H, Li J, Qiao X, et al. Sigma-1 receptor activation mediates the sustained antidepressant effect of ketamine in mice via increasing BDNF levels. Acta Pharmacol Sin [Internet]. 2024 [cited 5 October 2025]; 45: 704–13. Available at: https://www.nature.com/articles/s41401-023-01201-8

39. Ito H, Uchida T, Makita K. Ketamine Causes Mitochondrial Dysfunction in Human Induced Pluripotent Stem Cell-Derived Neurons. Franco R, Ed. PLOS ONE [Internet]. 2015 [cited 14 June 2025]; 10: e0128445. Available at: https://dx.plos.org/10.1371/journal.pone.0128445

40. Wan L-B, Levitch CF, Perez AM, et al. Ketamine Safety and Tolerability in Clinical Trials for Treatment-Resistant Depression. J Clin Psychiatry [Internet]. 2015 [cited 28 May 2025];

76: 247–52. Available at: https://www.psychiatrist.com/jcp/ketamine-safety-tolerability-clinical-trials-treatment

41. Lim J, Bang Y, Kim K-M, Choi HJ. Differentiated HT22 cells as a novel model for in vitro screening of serotonin reuptake inhibitors. Front Pharmacol [Internet]. 2023 [cited 16 March 2024]; 13. Available at: https://www.frontiersin.org/journals/pharmacology/articles/10.3389/fphar.2022.1062650/full

42. Divakaruni AS, Jastroch M. A practical guide for the analysis, standardization and interpretation of oxygen consumption measurements. Nat Metab [Internet]. 2022 [cited 21 March 2025]; 4: 978–94. Available at: https://www.nature.com/articles/s42255-022-00619-4

43. Dalwadi DA, Kim S, Schetz J, Schreihofer DA, Kim S. Brain-derived neurotrophic factor for high-throughput evaluation of selective Sigma-1 receptor ligands. J Pharmacol Toxicol Methods [Internet]. 2022 [cited 29 September 2025]; 113: 107129. Available at: https://linkinghub.elsevier.com/retrieve/pii/S1056871921001829

44. Knights KM, Stresser DM, Miners JO, Crespi CL. In Vitro Drug Metabolism Using Liver Microsomes. Curr Protoc Pharmacol [Internet]. 2016 [cited 14 June 2025]; 74. Available at: https://currentprotocols.onlinelibrary.wiley.com/doi/10.1002/cpph.9

45. Percie Du Sert N, Ahluwalia A, Alam S, et al. Reporting animal research: Explanation and elaboration for the ARRIVE guidelines 2.0. Boutron I, Ed. PLOS Biol [Internet]. 2020 [cited 29 September 2025]; 18: e3000411. Available at: https://dx.plos.org/10.1371/journal.pbio.3000411

46. Hong GP, Kim M-H, Kim HJ. Sex-related Differences in Glial Fibrillary Acidic Protein-positive GABA Regulate Neuropathology Following Pilocarpine-induced Status Epilepticus. Neuroscience [Internet]. 2021 [cited 29 September 2025]; 472: 157–66. Available at: https://linkinghub.elsevier.com/retrieve/pii/S0306452221003997

47. Buckmaster PS, Haney MM. Factors affecting outcomes of pilocarpine treatment in a mouse model of temporal lobe epilepsy. Epilepsy Res [Internet]. 2012 [cited 29 September 2025]; 102: 153–9. Available at: https://linkinghub.elsevier.com/retrieve/pii/S0920121112001684

48. Velíšková J, DeSantis KA. Sex and hormonal influences on seizures and epilepsy. Horm Behav [Internet]. 2013 [cited 29 September 2025]; 63: 267–77. Available at: https://linkinghub.elsevier.com/retrieve/pii/S0018506X12001079

49. Hesdorffer DC, Logroscino G, Cascino G, Annegers JF, Hauser WA. Incidence of status epilepticus in Rochester, Minnesota, 1965-1984. Neurology [Internet]. 1998 [cited 13 October 2025]; 50: 735–41. Available at: https://www.neurology.org/doi/10.1212/WNL.50.3.735

50. Leem Y-H, Park J-S, Park J-E, Kim D-Y, Kim H-S. Neurogenic effects of rotarod walking exercise in subventricular zone, subgranular zone, and substantia nigra in MPTP-induced

Parkinson's disease mice. Sci Rep [Internet]. 2022 [cited 21 July 2026]; 12: 10544. Available at: https://www.nature.com/articles/s41598-022-14823-5

51. Young K, Morrison H. Quantifying Microglia Morphology from Photomicrographs of Immunohistochemistry Prepared Tissue Using ImageJ. J Vis Exp [Internet]. 2018 [cited 14 June 2025]; 57648. Available at: https://app.jove.com/t/57648

52. Esteves M, Almeida AM, Silva J, et al. MORPhA Scale: Behavioral and electroencephalographic validation of a rodent anesthesia scale. J Neurosci Methods [Internet]. 2019 [cited 16 October 2025]; 324: 108304. Available at: https://linkinghub.elsevier.com/retrieve/pii/S0165027019301542

53. Statement on Continuum of Depth of Sedation: Definition of General Anesthesia and Levels of Sedation/Analgesia [Internet]. Committee on Quality Management and Departmental Administration, American association of anesthesiologists; 2024 [cited 2 January 2024]. Available at: https://www.asahq.org/standards-and-practice-parameters/statement-on-continuum-of-depth-of-sedation-definition-of-general-anesthesia-and-levels-of-sedation-analgesia

54. Martin BS, Kapur J. A combination of ketamine and diazepam synergistically controls refractory status epilepticus induced by cholinergic stimulation. Epilepsia [Internet]. 2008 [cited 3 March 2025]; 49: 248–55. Available at: https://onlinelibrary.wiley.com/doi/10.1111/j.1528-1167.2007.01384.x

55. Shivani, Singh G, Narwal S, Balram, Chopra B, Dhingra AK. Nano-formulations for the Management of Epilepsy: Synthetic and Herbal Drug Perspectives. Curr Nanomedicine [Internet]. 2024 [cited 3 March 2025]; 15. Available at: https://www.eurekaselect.com/235676/article

56. Vavers E, Zvejniece L, Dambrova M. Sigma-1 receptor and seizures. Pharmacol Res [Internet]. 2023 [cited 25 September 2025]; 191: 106771. Available at: https://linkinghub.elsevier.com/retrieve/pii/S1043661823001275

57. Pérez-Pérez D, Monío-Baca C, Von Rüden E, et al. Preclinical efficacy profiles of the sigma-1 modulator E1R and of fenfluramine in two chronic mouse epilepsy models. Epilepsia [Internet]. 2024 [cited 29 September 2025]; 65: 2470–82. Available at: https://onlinelibrary.wiley.com/doi/10.1111/epi.18037

58. Nguyen L, Lucke-Wold BP, Mookerjee S, Kaushal N, Matsumoto RR. Sigma-1 Receptors and Neurodegenerative Diseases: Towards a Hypothesis of Sigma-1 Receptors as Amplifiers of Neurodegeneration and Neuroprotection. In: Smith SB, Su T-P, Eds. Sigma Receptors: Their Role in Disease and as Therapeutic Targets [Internet]. Cham: Springer International Publishing; 2017 [cited 29 September 2025]: 133–52. (Advances in Experimental Medicine and Biology; vol. 964). Available at: http://link.springer.com/10.1007/978-3-319-50174-1_10

59. Liaw K, Zhang F, Mangraviti A, Kannan S, Tyler B, Kannan RM. Dendrimer size effects on the selective brain tumor targeting in orthotopic tumor models upon systemic

administration. Bioeng Transl Med [Internet]. 2020 [cited 5 October 2025]; 5: e10160. Available at: https://aiche.onlinelibrary.wiley.com/doi/10.1002/btm2.10160

60. Golub D, Yanai A, Darzi K, Papadopoulos J, Kaufman B. Potential Consequences of High-Dose Infusion of Ketamine for Refractory Status Epilepticus: Case Reports and Systematic Literature Review. Anaesth Intensive Care [Internet]. 2018 [cited 3 March 2025]; 46: 516–28. Available at: https://journals.sagepub.com/doi/10.1177/0310057X1804600514

61. US Food and Drug Administration. FDA approves new nasal spray medication for treatment-resistant depression; available only at a certified doctor's office or clinic. Press Htm. 2019;

62. Hu Y, Xu N, Li X, et al. Microtopography enhances intestinal drug absorption via Piezo1-mediated tight junction modulation. BMEMat [Internet]. 2026 [cited 25 July 2026]; 4: e70052. Available at: https://onlinelibrary.wiley.com/doi/10.1002/bmm2.70052

63. Movahedpour A, Taghvaeefar R, Asadi-Pooya A, et al. Nano-delivery systems as a promising therapeutic potential for epilepsy: Current status and future perspectives. CNS Neurosci Ther [Internet]. 2023 [cited 14 June 2025]; 29: 3150–9. Available at: https://onlinelibrary.wiley.com/doi/10.1111/cns.14355

64. Tang Q, Li D, Chen J, et al. Ultrasound Active Piezoelectric Nanostimulators for Long-Acting Wireless Deep Brain Electric Stimulation to Inhibit Epileptic Seizures. Adv Mater [Internet]. 2026 [cited 25 July 2026]; 38: e20447. Available at: https://advanced.onlinelibrary.wiley.com/doi/10.1002/adma.202420447

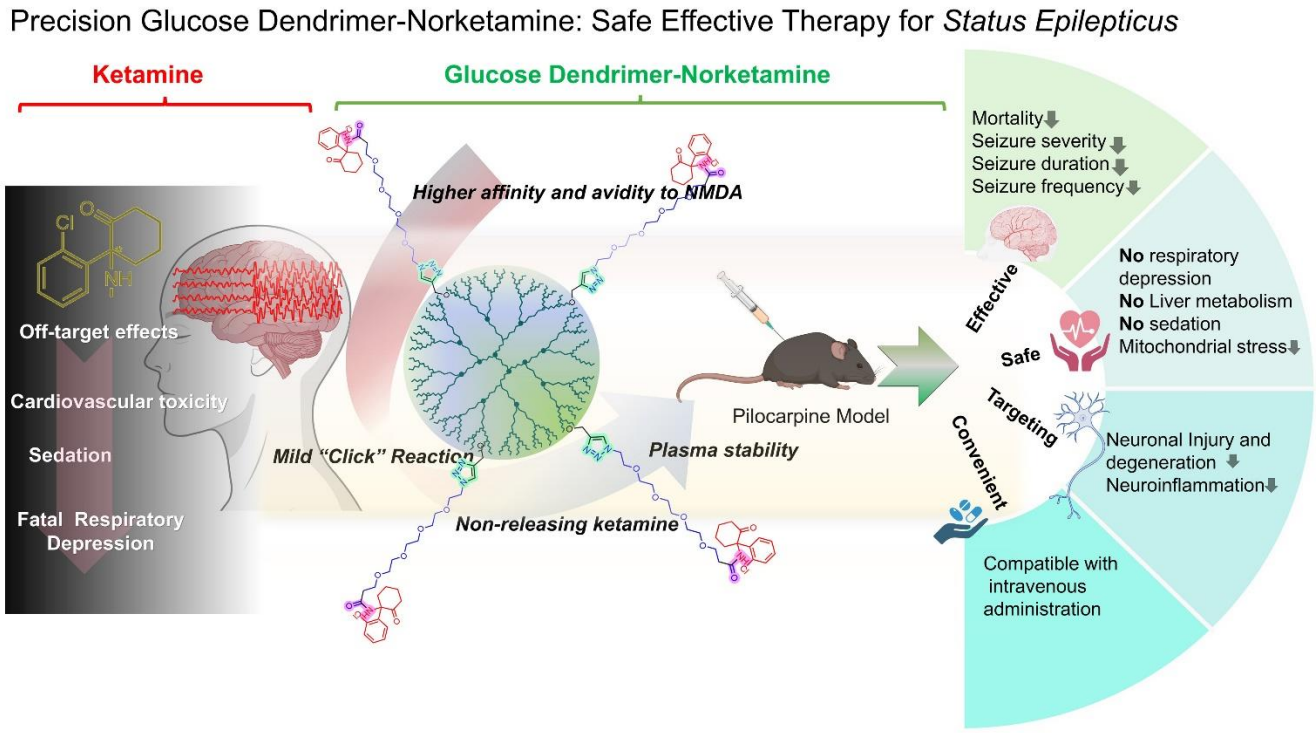
65. Hirano S, Bovi M, Romeo A, Guzzo F, Chiamulera C, Perduca M. Ketamine nano-delivery based on poly-lactic-co-glycolic acid (PLGA) nanoparticles. Appl Nanosci [Internet]. 2018 [cited 29 September 2025]; 8: 655–63. Available at: http://link.springer.com/10.1007/s13204-018-0765-1

66. Han FY, Liu Y, Kumar V, et al. Sustained-release ketamine-loaded nanoparticles fabricated by sequential nanoprecipitation. Int J Pharm [Internet]. 2020 [cited 29 September 2025]; 581: 119291. Available at: https://linkinghub.elsevier.com/retrieve/pii/S0378517320302751

67. Purohit MP, Yu BJ, Roy KS, et al. Acoustically activatable liposomes as a translational nanotechnology for site-targeted drug delivery and noninvasive neuromodulation. Nat Nanotechnol [Internet]. 2025 [cited 29 September 2025]; Available at: https://www.nature.com/articles/s41565-025-01990-5

68. Ge J, Tan R, Gao Q, et al. A Multifunctional Nanocarrier System for Highly Efficient and Targeted Delivery of Ketamine to NMDAR Sites for Improved Treatment of Depression. Adv Healthc Mater [Internet]. 2023 [cited 29 September 2025]; 12: 2300154. Available at: https://onlinelibrary.wiley.com/doi/10.1002/adhm.202300154

Graphical abstract



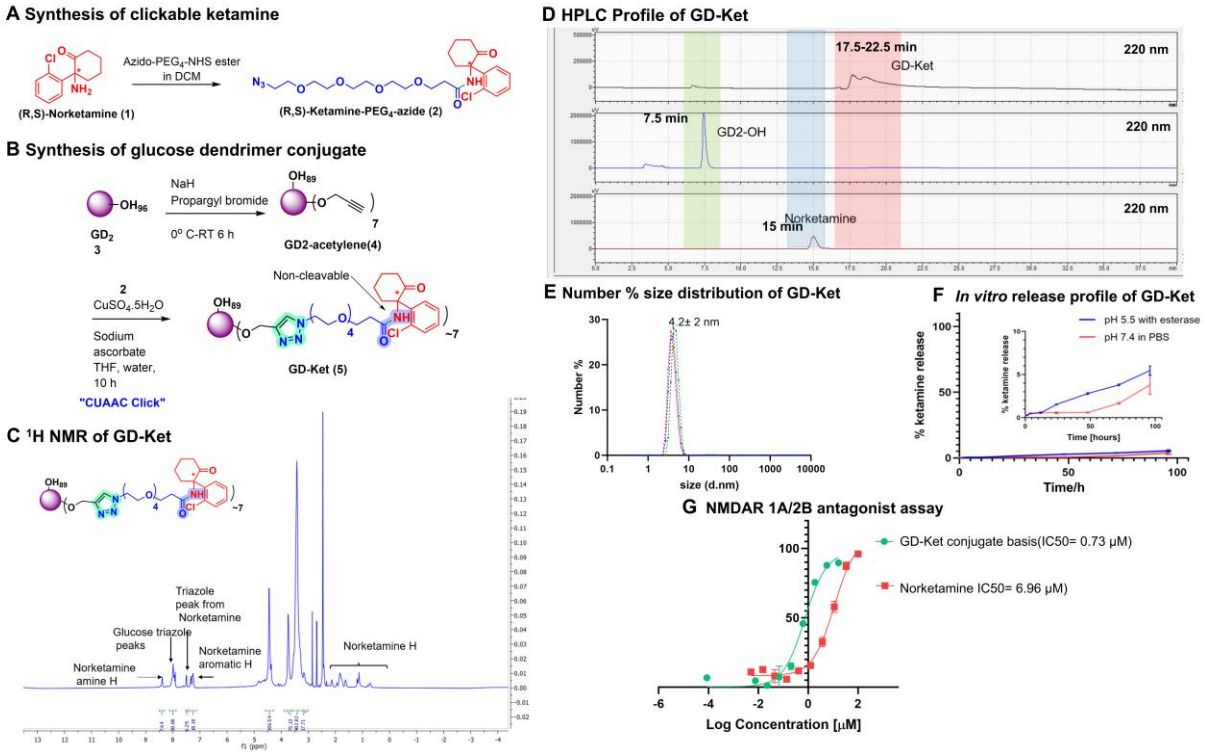


Figure 1. Synthesis and characterization of GD-Ket and synthetic intermediates. (B) Synthesis of the clickable ketamine conjugate, starting from a racemic mixture of Norketamine, **1**. The NHS-PEG_4-Azide reacted with compound **1** in DCM at RT to form compound **2**. (b) GD2 was partially functionalized with acetylene groups (~7) using NaH and propargyl bromide conditions. (R, S)-Norketamine-PEG_4-azide was conjugated to GD2 using a Cu(I) catalyzed click (CuAAC) reaction in the presence of a catalytic amount of $CuSO_4.5H_2O$ and sodium ascorbate to obtain GD-Ket. The subscripted numbers in the formulas indicate the number of acetylene, ketamine per dendrimer, (C) ^1H NMR (DMSO-*d6*, 500 MHz) characterization of GD-Ket, (D) HPLC profiles of key intermediates and final GD-Ket, (E) Zeta potential charge distribution of GD-Ket, (f) Number % size distribution GD-Ket, (G) the functional response of GD-Ket (indicated in green) to NMDAR 1A/2B ion channel blockage. The displacement curves show the concentration-response relationship compared to norket (red) and GD-Ket (red) on a conjugate basis (10% drug loading). (H) The *in vitro* drug release profile of GD-Ket demonstrates the conjugate's stability in both plasma and intracellular environments. IC_{50}: concentration of inhibitor required to reduce biological activity by 50%.

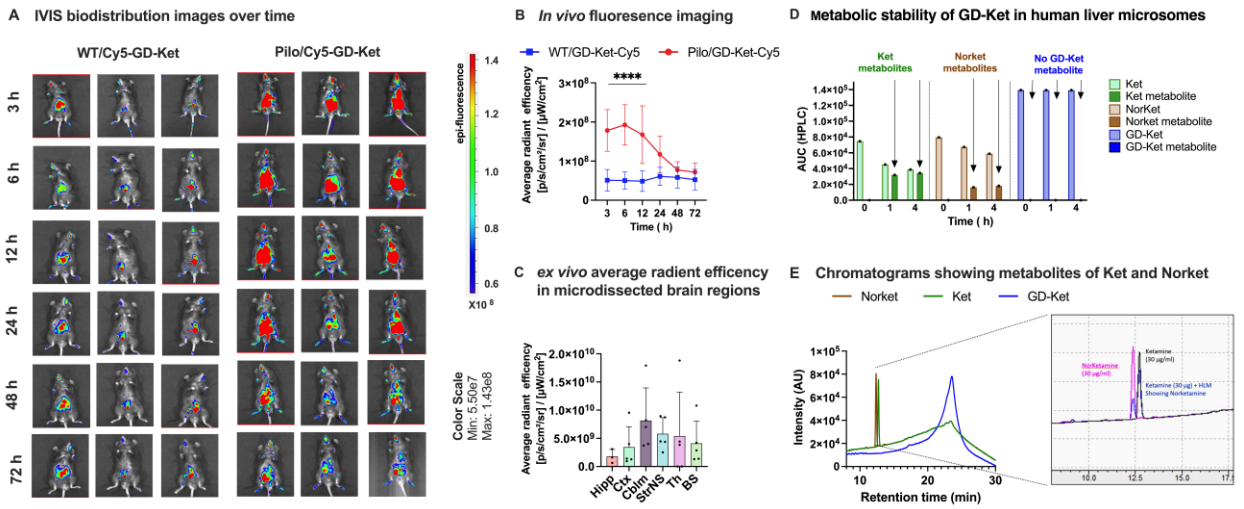


Figure 2. Biodistribution of Cy5-GD-Ket and metabolic stability of GD-Ket. (A) *In vivo* biodistribution and circulation of Cy5-GD-Ket in healthy versus pilocarpine-induced mice using IVIS Spectrum imaging. (B) Quantification of average radiant efficiency in pilocarpine-induced and healthy mice; (C) *ex vivo* average radiant efficiency of the micro-dissected brain regions in pilocarpine-induced mice. Average radiant efficiency is not measurable in the brain regions of healthy animals at this point; no signal was detected. (D-E) Assessment of metabolic stability of ketamine, norketamine, and GD-Ket via HPLC analysis following incubation with human liver microsomes (HLM) over 4 h. GD-Ket exhibits minimal metabolism, reflecting enhanced stability due to dendrimer conjugation with the parent drug, while metabolites are detected by HPLC at 1 and 4 h. Hipp: Hippocampus, Ctx: Cortex, Cblm: Cerebellum; StrNS: Striatum; Th: Thalamus; BS: Brainstem. Data represented as mean ± SD; n = 5/group. ****p < 0.0001 WT/Cy5-GD-Ket versus Pilo/Cy5-GD-Ket.

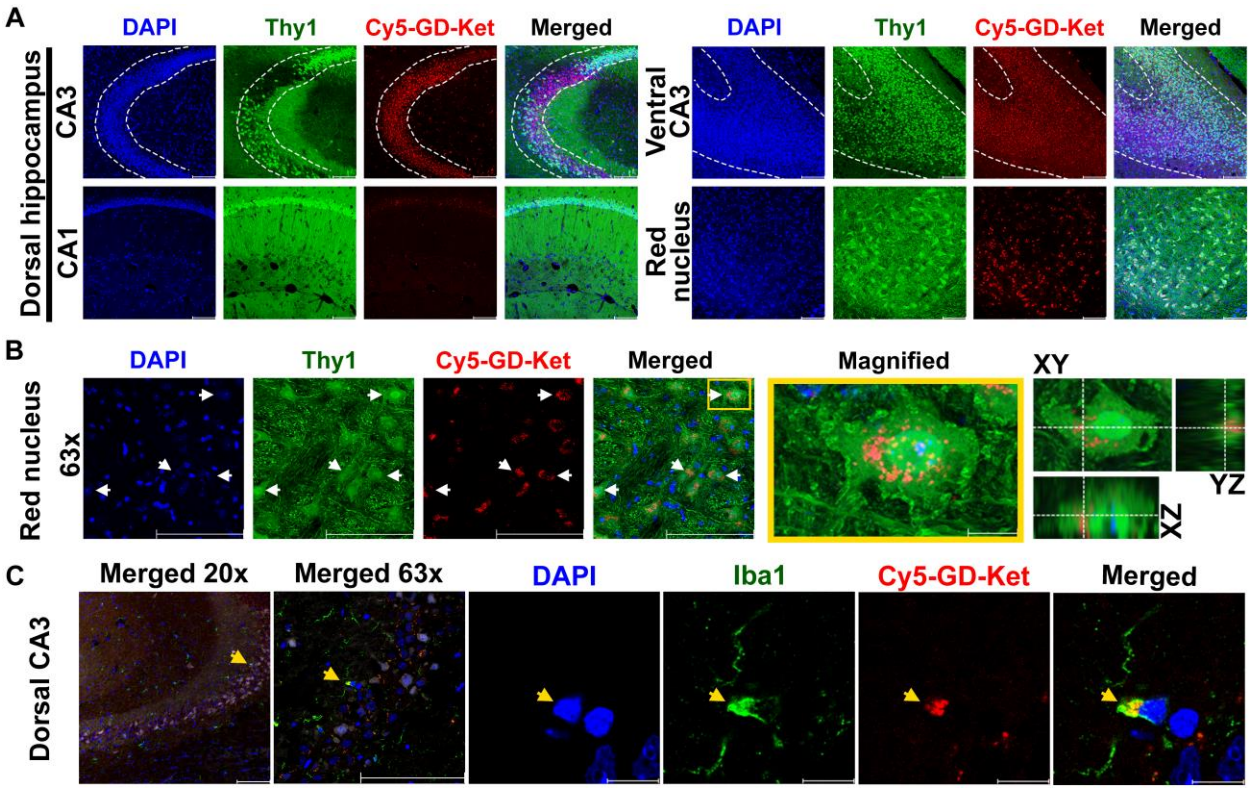


Figure 3. Cy5-GD-Ket localizes to neurons and microglia in the hippocampus and to neurons in the red nucleus in the midbrain upon IP administration in pilocarpine-induced mice with SE, at 4 h post-injection. (A) Confocal images of sections show localization of Cy5-GD-Ket within neurons (green, expressing Thy1-GFP label) in different regions, including dorsal & ventral CA3 regions (delineated by white broken lines) and red nucleus (20x); (B) Distribution of Cy5-GD-Ket in neurons of the red nucleus (63x max projection) (white arrows) and magnification of the cells to show internalization of the conjugate. We observed co-localization in the neurons by orthogonal sectioning of the acquired z-stacks, and (C) GD-Cy5 (Red) is also taken up by microglia (Iba1 staining, green) in the CA3 region of the hippocampus at 20X and 63X post-administration. Scale bar: 20 μm.

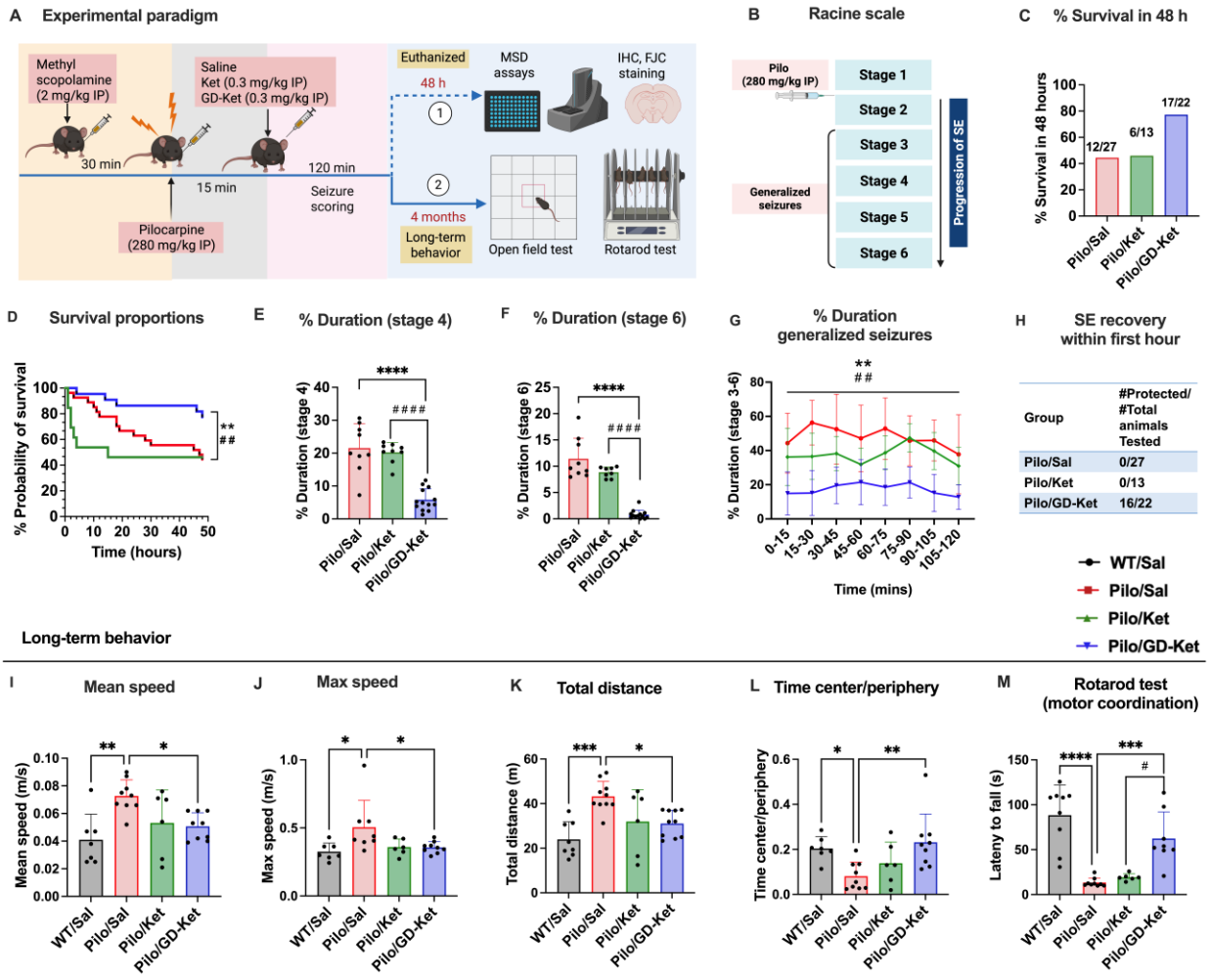


Figure 4. Efficacy of GD-Ket in pilocarpine-induced *status epilepticus (SE)*. (A) Experimental paradigm; (B) SE progression (C) GD-Ket improved % survival at 48 h post-SE; (D) survival proportions; GD-Ket-treated animals spent less time in higher seizure stages; GD-Ket reduced (E) % duration of stage 4 and (F) stage 6 seizures over 120 min, which are most associated with mortality; (E-G) GD-Ket and Ket reduced the duration of seizures in stage 3 and above in the first 120 min; however, GD-Ket was more effective in lowering higher stages of seizures over time; (H) Recovery from unceasing SE within the first hour of induction. Single-dose GD-Ket treatment administered during SE preserved locomotor activity and motor coordination at 4 months post-SE. (I-J) Increased mean and max velocity in the open field across trial durations indicated a distinct hyperactive phenotype in saline-treated mice at 4 months. GD-Ket treatment preserved locomotor activity compared to saline and ketamine. (K) GD-Ket treatment normalized hyperactivity-like behavior in these mice. (L) GD-Ket-treated animals spent more time in the center than in the peripheral zone and showed attenuated anxiety-like behavior post-SE. Saline- and ketamine-treated animals spent significantly less time in the center and remained localized to the periphery. This demonstrates that acute GD-Ket treatment rescues long-term hyperactivity and anxiety-like behavior in the open field. (M) GD-Ket improved long-term motor coordination at 4 months post-SE; it increased latency to fall (s) across accelerating trials in the rotarod test, demonstrating severe motor coordination deficits in saline- and ket-treated groups that are not seen with GD-Ket. Data are represented as mean ± SD. ****p < 0.0001, ** < 0.01, *p < 0.05 versus Pilo/Sal, $^{\#}$p < 0.05, $^{\#\#}$p < 0.01 versus Pilo/Ket and $^{\#\#\#\#}$p < 0.0001 versus Pilo/Ket.

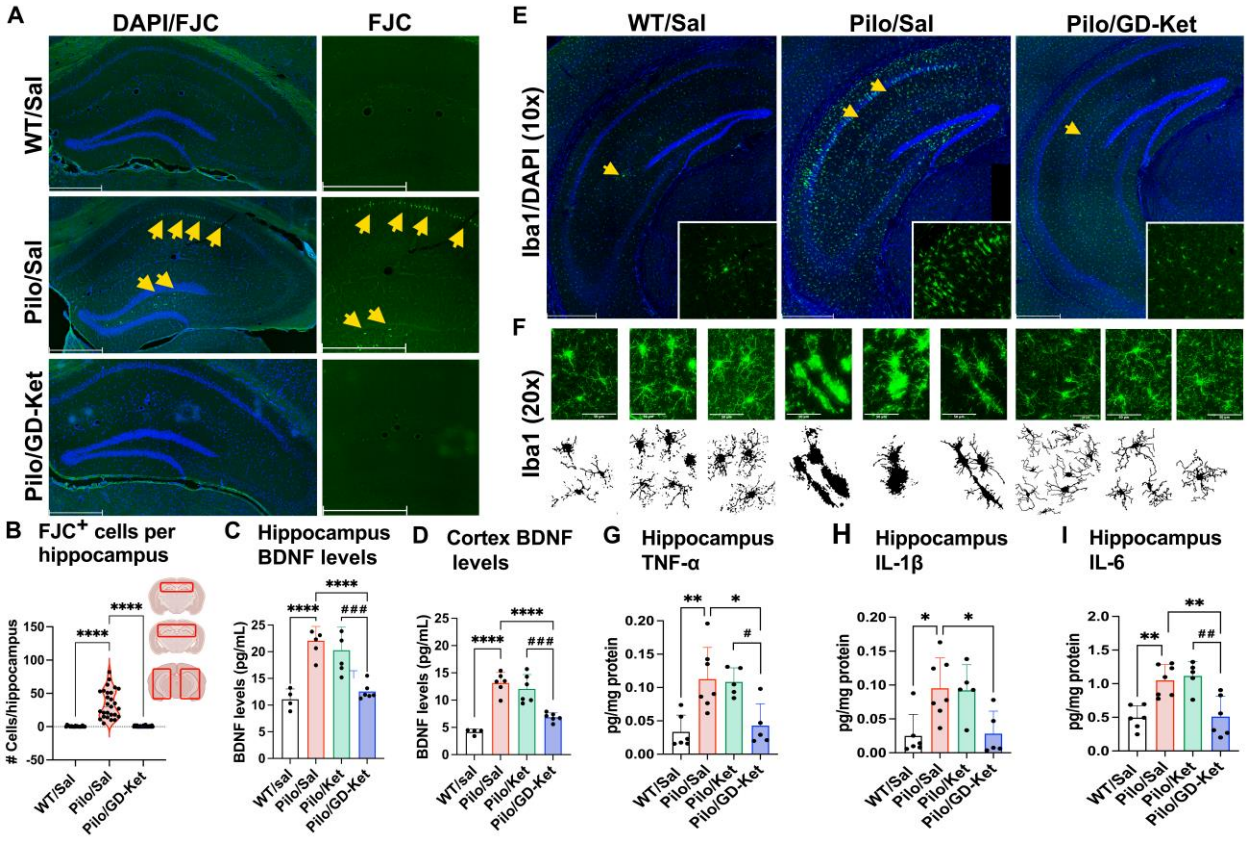


Figure 5. IHC analysis of GD-Ket efficacy at 48 h *post-SE*. GD-Ket-treated mice showed reduced neuronal neurodegeneration 48 h post-pilocarpine-induced SE. (A) Representative images of FJC-stained brain sections at 10X from C57BL/6 mice. Enlarged views of the hippocampal CA1 region showing greater numbers of FJC-stained neurons (yellow arrows) in saline-treated pilocarpine-induced mice versus GD-Ket. Free ketamine also reduced hippocampal cell death to some extent. However, the magnitude of improvement is higher in the GD-Ket-treated groups (scale bar: 500 µm). (B) FJC-stained neurons were significantly reduced in both Ket- and GD-Ket-treated mice (n = 3 per group) 48 h after *status epilepticus*. Schematics show the region of interest assessed, (C) BDNF levels in the hippocampus and (D) in the cortex. The hippocampal region shows increased neuroinflammation (Iba1 immunoreactivity, green) in a pilocarpine model of SE treated with saline and Ket but not in GD-Ket-treated mice (n=3). (E) Representative microglia morphology (20x) shows rod-shaped, bushy, and hypertrophic microglia in saline- and Ket-treated pilocarpine-induced mice (scale bar: 500 µm). (F) ImageJ tracings confirmed decreased microglial activation and morphology, showing only a few bushy microglia with predominant ramified microglia in GD-Ket-treated mice. (G-I) GD-Ket (0.3 mg/Kg) significantly reduced proinflammatory cytokines in the hippocampus 48 h post-injury, whereas Ket did not (n = 5-7). *** $p < 0.001$, ** $p < 0.01$ and * $p < 0.05$. BDNF: brain-derived neurotrophic factor, FJC: FluoroJade C.

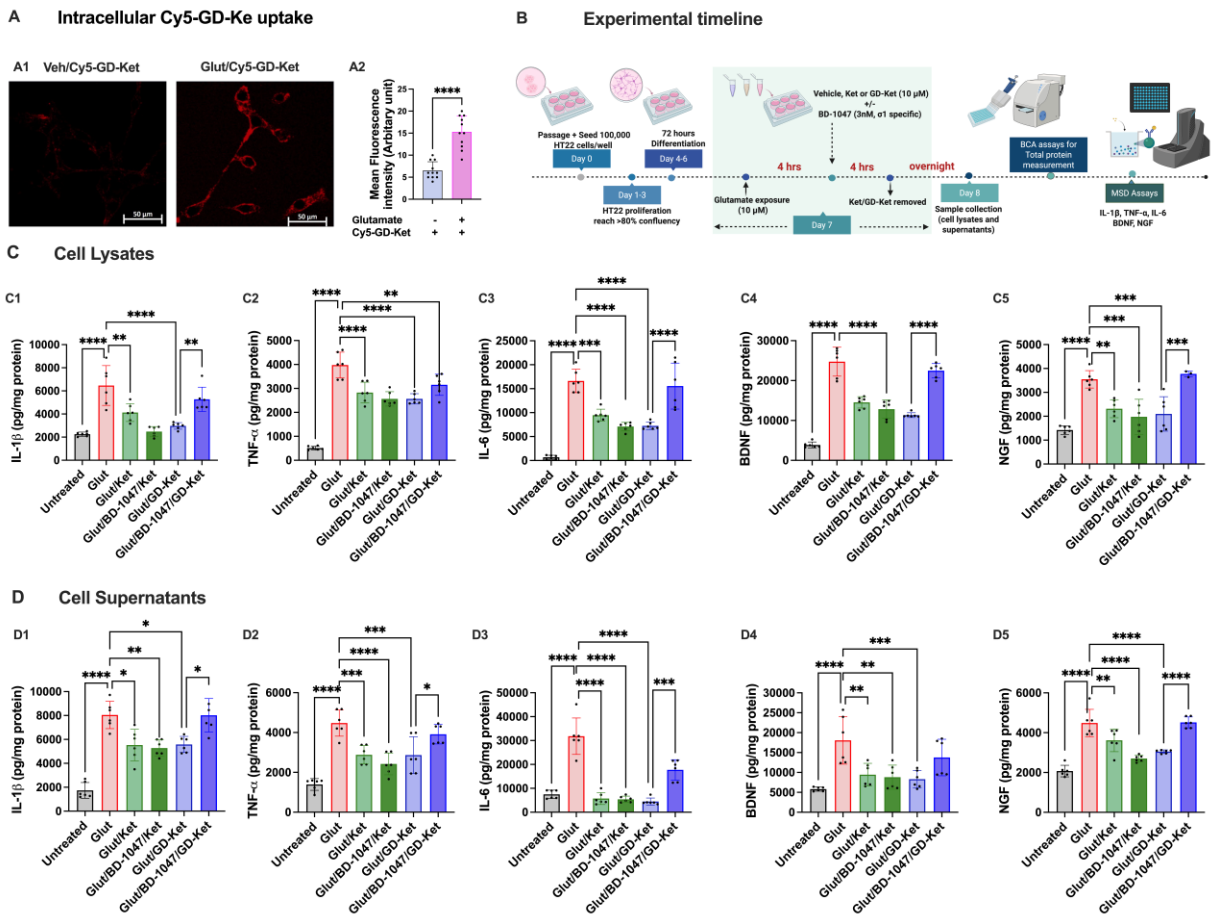


Figure 6: GD-Ket localizes intracellularly and exerts neuroprotective and anti-inflammatory effects through σ chaperone protein modulation. (A1) Confocal images of differentiated HT-22 cells, preincubated with vehicle (Veh) or glutamate (100 μM) for 4 h and subsequently treated with Cy5-Cy5-GD-Ket (20 μg/ml) for 24 h, are presented. Red indicates Cy5-GD-Ket. Images indicate the presence of Cy5-GD-Ket in the intracellular perinuclear and neurite region of the cell. (A2) quantitative analysis of Cy5-GD-Ket uptake by HT-22 cells. (B) Experimental timeline for pharmacological inhibition studies. (C-D) GD-Ket reduced the levels of cytokines, BDNF, and NGF in the glutamate-treated cell lysates and supernatants. However, this effect was blocked by σ1-antagonism, suggesting the involvement of σ1 chaperone modulation by GD-Ket. We did not observe a similar pattern with ketamine; it did not block or alter ketamine's pharmacological effects. **** $p < 0.0001$, *** $p < 0.001$, **$p < 0.01$ and *$p < 0.05$; N = 6wells/group. Glut: Glutamate, Ket: Ketamine, GD-Ket: GD-Ketamine, Veh: Vehicle.

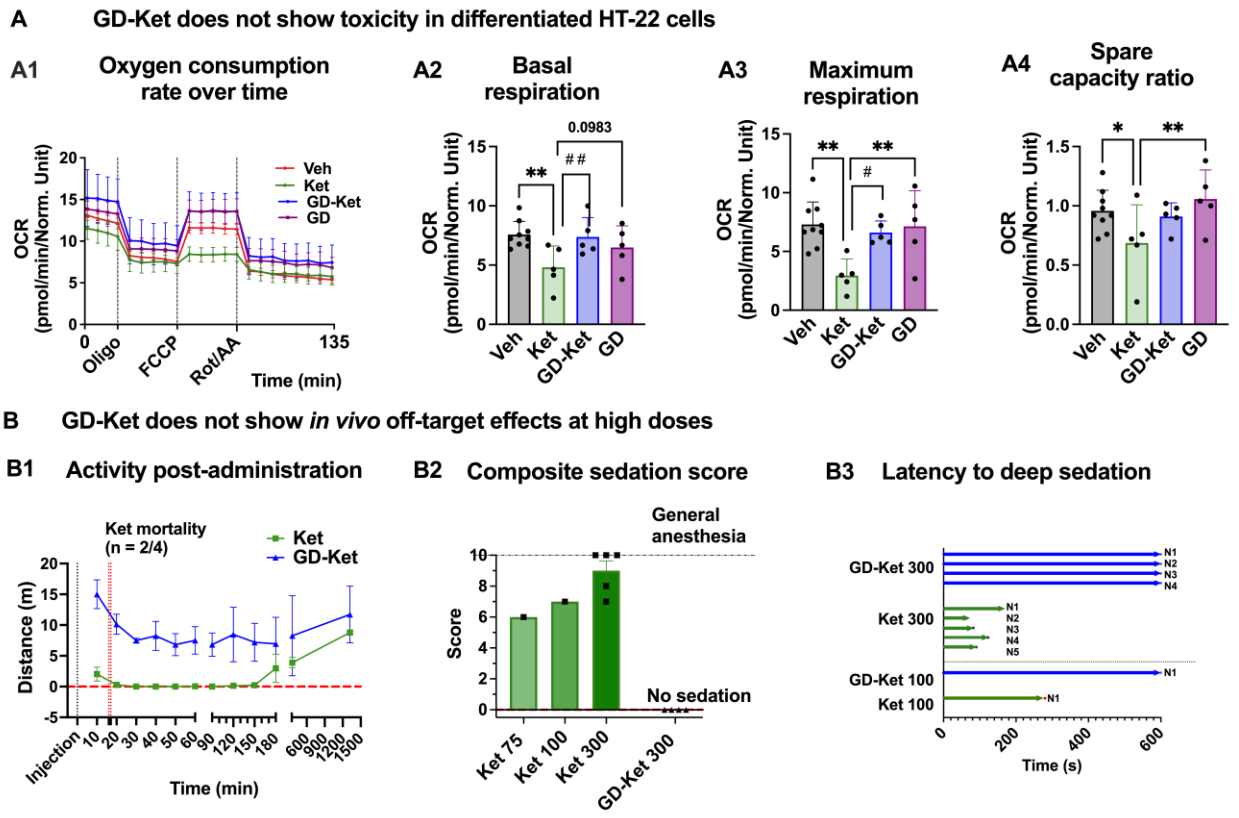


Figure 7. GD-Ket treatment had no toxic effects *in vitro* and *in vivo,* unlike free ketamine. (A) Real-time mitochondrial respiration was measured by determining (A1) oxygen consumption rate (OCR) using a Seahorse XF96 analyzer. Quantification of (A2) basal respiration, (A3) maximum respiration, and (A4) spare respiratory capacity when compared to saline vehicle control cells. GD-Ket and GD alone did not affect mitochondrial respiration or induce mitochondrial stress, unlike free ketamine. (B) High doses of GD-Ket do not induce immobility or inability to walk, sedation, or fatal respiratory depression/deep sedation requiring respiratory support, even at 300 mg/kg IP, represented as (B1) distance traveled at different time points post-administration of the drug, (B2) composite sedation score, and (B3) latency or time taken to go into deep sedation. Ketamine-induced dose-dependent immobility, ataxia, and respiratory distress are quantified as a composite sedation score (0 indicates no sedation; higher scores indicate more significant sedation and worse outcomes), with n=3-5 replicates/group. Oligo: oligomycin; FCCP: carbonyl cyanide-p-trifluoromethoxyphenylhydrazone; Rot: rotenone; AA: antimycin A. Data are represented as mean ± SD; n = 5/group. **** p<0.0001, *** p<0.001, ** p<0.01.